Volume 1 | Number 1 | Jan 2013 | Pages 1–100

PCCP

Physical Chemistry Chemical Physics
www.rsc.org/pccp

ROYAL SOCIETY OF CHEMISTRY

ROYAL SOCIETY OF CHEMISTRY

www.rsc.org/pccp

PCCP

Dynamic Article Links ▶

ARTICLE TYPE

Bond angle variations in XH₃ [X=N,P,As,Sb,Bi]: the critical role of Rydberg orbitals exposed using a diabatic state model

Jeffrey R. Reimers[ab]*, Laura K. McKemmish,[cd] Ross H. McKenzie,[e] and Noel S. Hush[df]

Ammonia adopts sp^3 hybridization (HNH bond angle 108°) whereas the other members of the XH₃ series PH₃, AsH₃, SbH₃, and BiH₃ instead prefer octahedral bond angles of 90-93°. We use a recently developed general diabatic description for closed-shell chemical reactions, expanded to include Rydberg states, to understand the geometry, spectroscopy and inversion reaction profile of these molecules, fitting 10 its parameters to results from Equation of Motion Coupled-Cluster Singles and Doubles (EOM-CCSD) calculations using large basis sets. Bands observed in the one-photon absorption spectrum of NH₃ at 18.3 eV, 30 eV, and 33 eV are reassigned from Rydberg (formally forbidden) double excitations to valence single-excitation resonances. Critical to the analysis is the inclusion of *all three* electronic states in which two electrons are placed in the lone-pair orbital n and/or the symmetric valence σ* antibonding 15 orbital. An illustrative effective two-state diabatic model is also developed containing just three parameters: the resonance energy driving the high-symmetry planar structure, the reorganization energy opposing it, and HXH bond angle in the absence of resonance. The diabatic orbitals are identified as sp hybrids on X; for the radical cations XH₃⁺ for which only 2 electronic states and one conical intersection are involved, the principle of *orbital following* dictates that the bond angle in the absence of resonance is 20 $\mathrm{acos}(-1/5) = 101.5°$. The multiple states and associated multiple conical intersection seams controlling the ground-state structure of XH₃ renormalize this to $\mathrm{acos}[3\sin^2(2^{1/2}\mathrm{atan}(1/2))/2 - 1/2] = 86.7°$. Depending on the ratio of the resonance energy to the reorganization energy, equilibrium angles can vary from these limiting values up to 120°, and the anomalously large bond angle in NH₃ arises because the resonance energy is unexpectedly large. This occurs as the ordering of the lowest Rydberg orbital and the 25 σ* orbital swap, allowing Rydbergization to compresses σ* to significantly increase the resonance energy. Failure of both the traditional and revised versions of the valence-shell electron-pair repulsion (VSEPR) theory to explain the ground-state structures in simple terms is attributed to exclusion of this key physical interaction.

1. Introduction

30 In the 1930's, following very quickly after the introduction of quantum mechanics, came what are now known as "diabatic" models for chemical reactions.[1-6] Diabatic surfaces provide mathematical representations of simple chemical ideas like ions and radicals, describing real molecules as mixtures of these basic 35 concepts: e.g., mixing purely ionic and purely covalent diabatic surfaces of water makes the polar bonds of the ground-state and simultaneously determines associated excited-state properties. Similarly, independent diabatic potential-energy surfaces are used to represent reactants and products of chemical reactions, and the 40 mixing of these surfaces produces transition states and also controls non-adiabatic processes.[7-9] These ideas proved extremely valuable in the 1950's, leading to the modern theory of electron transfer processes.[10-19] A critical feature of the diabatic approach has been its ability to unify a large range of ground-45 state chemical properties and excited-state spectroscopic properties,[20] leading to the field of charge-transfer spectroscopy[20, 21] and the subsequent understanding of how primary charge separation happens during photosynthesis and in its artificial

mimics.[22] In recent times, diabatic models have been applied to a 50 very wide range of chemical processes[23, 24] including aromaticity[25-29] and general chemical reactions,[23, 24, 30-32] being in particular very successfully applied to proton transfer processes.[33-44] Indeed, it is usual to describe all forms of pseudo Jahn-Teller[24, 45-47] and Herzberg-Teller[48] effects in this form.

55 However, general diabatic treatments have traditionally only shown partial success compared to the achievements of electron-transfer theory. Models have been shown to provide an excellent description of some significant chemical or spectroscopic property[24-29] but have failed to address the full range of treatable 60 properties using a single set of parameters. For example, diabatic models are extremely successfully used in looking at multidimensional reactions involving conical intersections including the *photodissociation* of NH₃ after excitation to its first electronically excited state.[49, 50] Such approaches explicitly 65 consider only the two states of immediate interest, however, excluding the manifold of inter-related states, and they are either not represented analytically or else involve a large number of parameters. Two-state diabatic approaches have also been described for the *inversion* reaction of ammonia and the XH₃

series, capturing the key physical insight but not leading to comprehensive analyses.[51]

Recently, we overcame the fundamental limitation concerning simple diabatic descriptions by demonstrating that electron-transfer reactions differ fundamentally from typical chemical processes as they involve radical species rather than closed-shell ones.[52] For radical reactions, only two states, the ground state and one excited state, can be produced from the frontier orbitals that control the chemical process. These two states are connected via a single conical intersection seam. While most chemical reactions occur at geometries far away from such seams, the presence of a seam usually dominates the energy landscape, giving rise to the reactant and product geometries and the properties of the transition state. For reactions of closed-shell species, the situation is quite different. The involvement of more than one electron in the reaction generates multiple coupled potential-energy surfaces made simply by specifying different occupations of the frontier orbitals. These surfaces display multiple conical intersection seams, and all seams qualitatively affect the geometric, spectroscopic, and kinetic properties.

Identifying the critical frontier orbitals giving rise to these states is the initial challenge facing diabatic analyses, with those specified by Valence-Bond theory being a good starting point.[53-55] The available valence orbitals are shown in Fig. 1 using NH_3 as an example: the NH symmetric bonding orbital σ_A, the degenerate bonding orbitals σ_E, the nonbonding HOMO orbital n, the symmetric antibonding orbital σ^*_A, and the degenerate bonding orbital σ_E. For the ammonia *inversion* reaction, the identified orbitals are σ_A, n, and σ^*_A. However, we have found that σ_A is only weakly involved and so can be ignored in the simplest diabatic approach,[52] justifying this usual and qualitatively very successful practice.[51, 56] The n to σ^*_A interaction thus generates 3 electronic states (the ground state G, the $n \rightarrow \sigma^*_A$ singly excited state S, and the $n \rightarrow \sigma^*_A, n \rightarrow \sigma^*_A$ doubly excited state D),
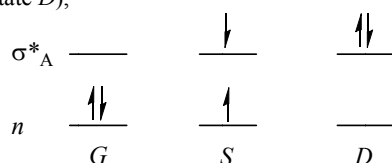
all of which are coupled together by the same strong vibronic coupling. For the Kekulé distortion of benzene, inclusion of the doubly degenerate HOMO and LUMO orbitals is required, generating 7 coupled electronic states.[52]

We have also shown that it is usually possible to introduce effective two-state models involving renormalized parameters that provide much simpler descriptions of molecular properties.[52] This makes available the wide range of results developed for electron-transfer theory and widely applied historically to more general problems, but the required parameter renormalization occurs in a property-dependent fashion.[52] This explains why previous generalized 2-state diabatic approaches have failed to be universal as different parameters are required to describe say the ground-state structure and the excited-state manifold. Using our modified theory it is possible, for example, to deduce diabatic C-C and C=C bond lengths of 1.53 Å and 1.31 Å, respectively, based on the observed value in benzene (1.41 Å) and excited-state spectral data only; similarly, we showed that, in crude calculations ignoring Rydberg states, it is possible to deduce the equilibrium bond angle and well depth for NH_3 inversion from spectroscopic data obtained at the planar geometry only.[52] Conversely, it is possible to estimate spectroscopic transition energies knowing only the shape of the ground-state potential-energy surface, and herein we analyze the latest full-dimensional

experimentally derived[57-60] and theoretical[61] surfaces as well as those produced from high quality calculations.
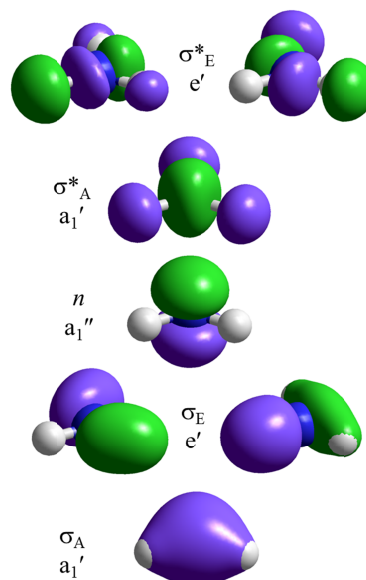
Our previous work focused on general principles appropriate to many reactions, interpreting calculated data obtained using minimal basis sets to avoid introducing interfering spectator chemical features;[52] NH_3 was chosen as one of the example systems. Here we consider the extended XH_3 series of molecules NH_3, PH_3, AsH_3, SbH_3, BiH_3, using high-level computational methods. These methods can quantitatively depict the properties of all states of the molecules of interest, providing comprehensive insight into the molecular chemical and spectroscopic properties. Our original 3-state diabatic model is expanded to a 6-state one, including all transitions associated with the lowest-lying X s Rydberg molecular orbital. While the calculations depict transitions involving many other Rydberg orbitals, inclusion of just this single orbital is found to be sufficient to allow for quantitative analysis. This is a significant result as, for NH_3 for example, the energies of the valence states of interest lie above not only the lowest (vertical) Rydberg transition $n \rightarrow 3s$, which is observed at 6.5 eV[62] and leads to the first ionization potential (IP) $n \rightarrow \infty$ at 10.9 eV,[63] but also the states associated with the IPs observed at 16.4 eV and 27.3 eV for the $\sigma_E \rightarrow \infty$ and $\sigma_A \rightarrow \infty$ ionizations, respectively.[64]

The simplest method for predicting qualitative molecular structure is valence-shell electron-pair repulsion (VSEPR) theory.[65-67] In its original form,[65] this predicts that XH_3 molecules containing a lone pair have 4 valence-shell electron pairs and thus adopt a basic tetrahedral electron-pair structure. However, lone-pairs occupy more angular area than do bonding electron pairs and hence HXH bond angles are predicted to be compressed below the tetrahedral value of acos(-1/3) = 109.5°. Ammonia has an angle of 107.5° and is (still) listed as a classic example of this effect.[67] However, substituted molecules like $N(SiH_3)_3$ can have no barrier[67] and be planar with 120° bond angles while PH_3, AsH_3, SbH_3, and BiH_3 have bond angles of 93°-90°, typical of octahedral coordination. The observation of angles near 90° is interpreted as being accidental and a result of the hydrogen ligands being equivalently (or even slightly excessively) electronegative compared to the central atom. As a

result, electrons are drawn to the ligands and hence the bonds occupy much smaller solid angles than does the lone pair. Also the planar molecule is similarly attributed to a large electronegativity difference pushing electrons onto the central atom, the problem being that an infinite electronegativity difference should generate 4 equivalent electron pairs and hence the limiting structure is actually tetrahedral.

In later developments of the VSEPR theory, the observed near 90° angle was initially attributed to bonding electron pairs not repelling until nearly this angle was reached,[66] leading to the modern version of the theory in which inter-ligand repulsions take on a central, semi-quantitative, role.[67] In this new approach, the bond angles of NH_3 - BiH_3 and $N(SiH_3)_3$ are determined purely by the "ligand radii" of the different XH bonds involved.[66] This analysis can be summarized simply in terms of an unstated principle: lone-pairs always expand to cover as much angular domain as possible, subject to the constraints imposed by the ligand radii. The native bonding pattern in this system is therefore octahedral (rather than tetrahedral as per the original VSEPR theory), with inter-ligand repulsions pushing the observed HXH angle out from 90°–93° for BiH_3–PH_3 to 107° for NH_3 and finally to 120° for $N(SiH_3)_3$. This interpretation also explains the structures[68] of related molecules like SiH_3^+ (bond angle 120°, no lone pair electrons so inter-ligand repulsions fully control the structure), SiH_3^- (bond angle 93°, two lone pair electrons expand to fill octahedral coordination sites until the ligand radii are engrossed upon), and $SiH_3^\bullet$ (bond angle 111°, one lone pair electron only partially pushes the ligands back).

While modern VSEPR theory can account for the ground-state structures of the XH_3 series, this description is complex and involves many specifically set parameters. The theory does not consider spectroscopic properties at all, however. Here, we seek a simpler, diabatic, description of the factors controlling spectroscopy and hybridization. It is based on the assumption that diabatic hybrid sp orbitals of form $2^{1/2}(\psi_s \pm \psi_p)$ on the central X atom change little in nature as a function of the torsional bending angle. Resonance-driven mixing of these orbitals that changes as a function of the torsional angle then simultaneously generates the well-known adiabatic lone-pair and σ^*_A orbital properties of the system. For XH_3^+, only one conical intersection seam controls the ground-state properties, and orbital following[69] and symmetry then demands that the equilibrium structure of the diabatic states has HXH angles oriented in the same directions as the XH bonding orbitals that form orthogonal to the sp hybrids. For XH_3, the presence of multiple seams renormalizes this angle, making it much smaller, however. Also, moving an electron between the diabatic orbitals in the presence of the hydrogens costs a considerable amount of energy, known as the reorganization energy. At its simplest level, once the effects of parameter renormalization are taken into account, understanding the properties of the XH_3 molecules and their radical cations in the diabatic description comes down to the determination of two properties: the resonance energy and the reorganization energy. However, the Rydberg states of NH_3 strongly interfere with the valence states in a process described by Mulliken as "Rydbergization",[70, 71] and its importance in determining the ground-state structure and well depth is revealed.

2. Methods

Ab initio electronic-structure calculations of potential-energy surfaces are performed using the MOLPRO package.[72] Two types of state energies are reported, those obtained using complete-active space self-consistent field (CASSCF) calculations with n electrons distributed amongst m orbitals,

$CAS(n,m)$,[73-75] and those obtained using equations of motion coupled-cluster singles and doubles theory (EOM-CCSD).[76, 77] The XH bond lengths R_{XH} are optimized for each structure using 2nd-order Møller-Plesset perturbation theory (MP2)[78] for the CASSCF calculations and the native CCSD method for the EOM-CCSD calculations. Some reference single-point calculations are also performed using perturbative corrections for triples, CCSD(T).[79] Also, spectroscopic calculations including transition moments are evaluated at equilibrium geometries by the SAC-CI method,[80] which is very similar to EOM-CCSD[81] using GAUSSIAN,[82] as well as by the semi-empirical complete neglect of differential overlap (CNDO) methods CNDO/S[83, 84] and CNDO/2,[88, 89] and the intermediate neglect of differential overlap (INDO) method INDO/S,[85] all using our own multi-reference configuration-interaction program.[86, 87]

A wide range of basis sets are used for calculations on NH_3 including the minimal basis STO-3G,[88] 6-31G*,[89] and the double-zeta to quad-zeta series cc-pVDZ, cc-pVTZ, and cc-pVQZ,[90-92] as well as the augmented and doubly augmented sets aug-cc-pVDZ, aug-cc-pVTZ, and d-aug-cc-pVDZ.[93] Always a compromise must be made between basis sets that reproduce experimental data to very high accuracy and those for which the results are easily interpretable. Mostly we are concerned with the description afforded of the valence states and of, in particular, the lowest Rydberg state. As the lowest Rydberg state involves considerable mixing with the valence states, it is found to be described at a useful level even by the 6-31G* basis. Augmented basis sets lead to the calculation of very many orbitals and states that are spectators to the processes of interest and therefore make analysis difficult. Hence for all molecules except NH_3 we use basis sets without augmented functions. STO-3G is used for P, As, and Sb and also cc-pVDZ[94] and cc-pV(T+d)Z[95] for P, and cc-pVDZ-PP and cc-pVTZ-PP for As, Sb, and Bi.[96] Also for, As, Sb, and Bi, the relativistic effective core potentials ECP10MDF, ECP28MDF, and ECP60MDF are used, respectively.[97] In addition, for N and As, the STO-3G basis set is augmented by a single s function with $\zeta = 0.07$ au and 0.045 au, respectively, in a basis we name aSTO3G. This provides a useful description of the nitrogen 3s Rydberg orbital and its associated spectroscopy, for example. High-quality single-point energy calculations on the ground states of all molecules are performed using the aug-cc-pwCVQZ basis for H, N, and P, and aug-cc-pwCVQZ-PP for As, Sb, and Bi.[90, 93, 98]

3. Results

a) The basic 3-state diabatic model and its parameters

We have shown that the simplest description of chemical reactions like XH_3 inversion involves a one-vibrational-dimensional model coupling the three diabatic electronic states G, S, and D.[52] Deduced from this model are then the related uncoupled adiabatic states g, s, and d, respectively. The diabatic states differ from the adiabatic ones in that their form is taken to be the same, independent of molecular geometry. How molecular distortion affects the electronic motions is then included as vibronic couplings. Application of the Born-Oppenheimer approximation to the Hamiltonian matrix expressed in terms of the diabatic states leads to the specification of the adiabatic ones. However, diabatic states are not unique[99] and may be transformed into many equivalent forms. While all possible forms lead to the same converged numerical solutions for system properties, different approaches highlight different key physical features and can have quite different convergence properties.[100] We also consider a key alternative form, the localized diabatic

description in which G, S, and D are transformed into states named L, C, and R corresponding to different equilibrium geometries: the left-hand side of a double-well potential for L (i.e., one pyramidal XH_3 structure), the central high-symmetry geometry for C (i.e., a planar structure), and the right-hand side of a double well R (i.e., the alternate pyramidal XH_3 structure). The adiabatic states, and all calculated molecular properties, are invariant to this transformation.

In detail, calculated molecular properties are sensitive not only to the 3 key diabatic states but also to any state that interacts with them at some geometry. If interactions with other states are profound then they need to be included explicitly, expanding the number of electronic states considered in the calculation. Indeed, we do this for the critical Rydberg states, as described in Section 3b. However, the influences of all other states are included implicitly by modifying other model parameters slightly. Herein this is done by fitting the model parameters to calculated surfaces, but automated computational methods such as those used in 2-state pseudo-Jahn-Teller theory[24] are available and can easily be generalized to treat multiple diabatic states.[101]

For the three key states, we expand the effects of nuclear motion on the diabatic states using a Taylor series expansion about the high-symmetry planar geometry, keeping all terms of up to fourth order. A total of 11 parameters appear in this expansion of which 5 are required at the most basic level of approximation and 6 depict higher-order corrections such as anharmonicities. For many chemical systems, treatment at the harmonic level is adequate but, for the inversion motion of XH_3 molecules, large amplitude motions are involved and hence inclusion of anharmonic contributions is essential. All of the parameters used in the model, and indeed all quantities discussed in this article, are compared and contrasted in detail in the Appendix..

The Hamiltonian is written in terms of the improper torsional angle[102, 103] τ that takes on a value of zero at the planar geometry. This is related to the HXH bond angle θ by

$$2\cos\theta = 3\sin^2\tau - 1 . \qquad (1)$$

The diabatic surfaces for G, S, and D have minima at the planar structure. The energies of these states differ and we represent the S-G and D-S differences as $2|J_G|$ and $2|J_D|$, respectively, where as we shall see later J_G and J_D are the associated *resonance integrals*. The shapes of the diabatic surfaces are represented by harmonic and quartic force constants k and k_4, respectively. At the most basic level all diabatic states have the same force constants, it being the vibronic coupling between them that leads to different force constants for the adiabatic states. However, interferences with nearby states can change the force constants, and so a general model must allow variations of the force constants of the G, S, and D states, here specified by parameters $2\beta_G$ and $2\beta_D$.

The key vibronic couplings are odd functions of the nuclear coordinate and so are represented in terms of integrals α_G and α_D specifying the associated G-S and S-D linear vibronic couplings $\alpha_G = \langle\Psi_G|\partial\mathbf{H}/\partial\tau|\Psi_S\rangle$ and $\alpha_D = \langle\Psi_D|\partial\mathbf{H}/\partial\tau|\Psi_S\rangle$, where $\mathbf{H}$ is the Hamiltonian operator. Anharmonic corrections are provided by the associated cubic couplings $\gamma_G = \langle\Psi_G|\partial^3\mathbf{H}/\partial\tau^3|\Psi_S\rangle$ and $\gamma_D = \langle\Psi_D|\partial^3\mathbf{H}/\partial\tau^3|\Psi_S\rangle$, respectively. Even though the G and D states have the same symmetry, they may still couple

through anharmonic interactions, the leading term of which is the second-order vibronic coupling $\beta = \langle\Psi_G|\partial^2\mathbf{H}/\partial\tau^2|\Psi_D\rangle$, and this term is also included.

The total Hamiltonian for this 3-state delocalized-diabatic model is named $\mathbf{H^{3D}}$ and in the $\{G,S,D\}$ basis has matrix elements

$$H_{G,G}^{3D} = T + \frac{k}{2}\tau^2 + \frac{k_4}{24}\tau^4$$

$$H_{S,S}^{3D} = T + \left(\frac{k}{2} + \beta_G\right)\tau^2 + 2|J_G| + \frac{k_4}{24}\tau^4$$

$$H_{D,D}^{3D} = T + \left(\frac{k}{2} + \beta_G + \beta_D\right)\tau^2 + 2|J_G| + 2|J_D| + \frac{k_4}{24}\tau^4$$

$$H_{G,S}^{3D} = \alpha_G\tau + \frac{\gamma_G}{6}\tau^3 \qquad (2)$$

$$H_{G,D}^{3D} = \frac{\beta}{2}\tau^2$$

$$H_{S,D}^{3D} = \alpha_D\tau + \frac{\gamma_D}{6}\tau^3$$

where in addition T is the kinetic energy operator

$$T = \frac{-\partial^2}{2\mu'\partial\tau^2} \qquad (3)$$

with μ' the associated moment of inertia (which is coordinate dependent).

The most fundamental parameters are J_G, J_D, α_G, α_D, and k, whilst k_4, β, β_G, β_D, γ_G, and γ_D are higher-order corrections. The same orbitals are involved in the processes that generate the two resonance energies and the two vibronic couplings and so the majority of the contributions leading to these integrals are in common and thus similar values are expected. However, at the simplest level, it is possible to approximate[52] $J_G = J_D$ and $\alpha_G = \alpha_D$, in which case the minimum number of required parameters is just three. Of the 6 higher-order corrections, β_G and β_D appear as empirical corrections to the force constant designed to treat implicitly the effects of additional states on the three states of interest. In practice, we find that the high-energy state D is often involved with resonances with other states, making it difficult to always isolate. Given this, we find the most practical solution to stable numerical fitting to be to set[52]

$$\beta = \beta_G = \beta_D = 0 , \qquad (4)$$

leaving just 8 free parameters to be fitted.

So as to understand the behaviour of Eq. (2) in the limit where the resonance integrals are small, we introduce the coordinate-independent transformation[52] of the $\{G,S,D\}$ delocalized diabatic electronic basis states to produce the localized diabatic basis states $\{L,C,R\}$. In this electronic basis, the original Hamiltonian $\mathbf{H^{3D}}$ is *equivalently* represented as $\mathbf{H^{3L}}$ where

$$H_{L,L}^{3L} = T - \frac{k(\tau_{mG} + \tau_{mD})^2}{4} + \frac{3J_G + J_D}{2} + \frac{k}{2}\left(\tau + \frac{\tau_{mG} + \tau_{mD}}{\sqrt{2}}\right)^2$$
$$+ \frac{\beta + 3\beta_G + \beta_D}{2}\tau^2 + \frac{(\gamma_G + \gamma_D)}{6\sqrt{2}}\tau^3 + \frac{k_4}{24}\tau^4$$

$$H_{C,C}^{3L} = T + J_G + J_D + \frac{k - \beta + \beta_G + \beta_D}{2}\tau^2 + \frac{k_4}{24}\tau^4 \qquad (5)$$

$$H_{R,R}^{3L} = T - \frac{k(\tau_{mG} + \tau_{mD})^2}{4} + \frac{3J_G + J_D}{2} + \frac{k}{2}\left(\tau - \frac{\tau_{mG} + \tau_{mD}}{\sqrt{2}}\right)^2$$
$$+ \frac{\beta + 3\beta_G + \beta_D}{2}\tau^2 - \frac{(\gamma_G + \gamma_D)}{6\sqrt{2}}\tau^3 + \frac{k_4}{24}\tau^4$$
$$H_{L,C}^{3L} = -\frac{(J_G + J_D)}{\sqrt{2}} + \frac{\alpha_G - \alpha_D}{2}\tau - \frac{\beta_G + \beta_D}{2\sqrt{2}}\tau^2 + \frac{\gamma_G - \gamma_D}{12}\tau^3$$
$$H_{L,R}^{3L} = \frac{J_G - J_D}{2} - \frac{\beta - \beta_G + \beta_D}{4}\tau^2$$
$$H_{C,R}^{3L} = \frac{(J_G + J_D)}{\sqrt{2}} + \frac{\alpha_G - \alpha_D}{2}\tau + \frac{\beta_G + \beta_D}{2\sqrt{2}}\tau^2 + \frac{\gamma_G - \gamma_D}{12}\tau^3$$

and

$$\tau_{mG} = \frac{\alpha_G}{k} \text{ and } \tau_{mD} = \frac{\alpha_D}{k} \quad . \qquad (6)$$

In the 5-parameter model in which all higher order corrections k_4, β, β_G, β_D, γ_G, and γ_D are ignored, the L and R localized diabatic surfaces have minima at

$$\tau = \pm\frac{\tau_{mG} + \tau_{mD}}{\sqrt{2}} \quad . \qquad (7)$$

If only two states (e.g., G and S or S and D) are involved, as is the case for the radical cations XH_3^+ and for most electron-transfer reactions, then the localized states would have minima at $\tau = \pm\tau_{mG}$ or $\pm\tau_{mD}$. It is therefore convenient to define harmonic reorganization energies as

$$\lambda_G = 2k\tau_{mG}^2 = \frac{2k\alpha_G^2}{k} \text{ and } \lambda_D = 2k\tau_{mD}^2 = \frac{2k\alpha_D^2}{k}. \qquad (8)$$

Note that the actual diabatic minima for XH_3 inversion are the renormalized quantities

$$\tau_{dmG} = \sqrt{2}\tau_{mG} \text{ and } \tau_{dmD} = \sqrt{2}\tau_{mD} \qquad (9)$$

from which related HXH bond angles θ_{dmG} and θ_{dmD} can be defined using Eqn. (1).

Important analytical expressions available for this model include those for the second and fourth derivatives of the adiabatic potential-energy surfaces at the planar D_{3h} geometry, as well as these inverted to give J_G, J_D, α_G, α_D, k, k_4, β, β_G, β_D, γ_G, and γ_D analytically in terms of the derivatives and associated state energies.[52] In this way, realistic descriptions of *all* of the complex anharmonic potential-energy surfaces can be obtained performing calculations at a *single geometry* only. This connection is what gives diabatic models their great power. Analytical derivatives are also available at the ground-state equilibrium geometry of double-welled potentials for use in interpreting observed spectroscopic data.[52]

b. Expansion to a 6-state model including Rydberg transitions

To include the effect of Rydberg transitions, this 3-state model is expanded to include all transitions associated with the lowest-lying Rydberg molecular orbital which is, for example, the nitrogen 3s orbital for NH_3:
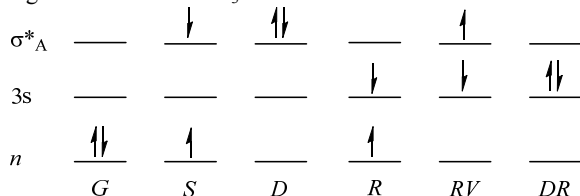
where the $n\rightarrow3s$ Rydberg excitation is named R, the $n\rightarrow3s,n\rightarrow3s$ double Rydberg excitation is named DR, and the $n\rightarrow\sigma^*_A,n\rightarrow3s$ combined Rydberg + valence excitation is named RV. Our diabatic analysis is performed at the level of electronic states rather than at the orbital level, however, and the quantum chemical calculations reveal already mixed orbitals, meaning that this notation, and the Hamiltonian functional form that comes with it, is only approximate. Nevertheless, in the expanded $\{G,S,D,R,RV,DR\}$ delocalized diabatic basis, the electronic Hamiltonian $\mathbf{H^{6D}}$ is $\mathbf{H^{3D}}$ augmented with the matrix elements

$$H_{R,R}^{6D} = H_{G,G}^{6D} + E_R$$
$$H_{RV,RV}^{6D} = H_{V,V}^{6D} + E_R + J_D - J_G$$
$$H_{DR,DR}^{6D} = 2H_{G,G}^{6D} + E_R + \Gamma_R \qquad (10)$$
$$H_{R,V}^{6D} = H_{DR,RV}^{6D} = H_{D,RV}^{6D} = V_{RV}$$

involves three new parameters, the unperturbed Rydberg state energy E_R, the on-site repulsion Γ_R between two electrons *occupying* the Rydberg orbital, and the Rydberg-valence interaction energy V_{RV}. Note that this functional form represents the electronic interactions for the mixed double excitation as the sum of half of those for the double-valence and double-Rydberg excitations, averaging the on-site repulsion energies. While this is a crude approximation in general, it appear to work very well for the XH_3 series and considerably simplifies identification of the correct assignments of the calculated data. Also, Eqn. (10) implies use of the same harmonic and anharmonic force constants for R, RV, and DR as used for G, S, and D. In principle, these force constants should *differ* as electrons are being taken from the lone-pair orbital to the Rydberg orbital, but as neither of these orbitals has bonding character, the effects are expected to be small. Hence to have a level of approximation consistent with Eqn. (4), such variations are neglected.

What results is thus a 6-state diabatic model containing 11 free parameters. Diagonalization of $\mathbf{H^{6D}}$ parametrically as a function of torsional angle leads to 6 adiabatic Born-Oppenheimer potential-energy surfaces. Using parameters appropriate for XH_3 inversion reactions, this process yields 6 surfaces with properties similar to those of the original $\{G,S,D,R,RV,DR\}$ diabatic basis states and so the adiabatic surfaces are accordingly named *g, s, d, r, rv,* and *dr*.

c) Reduction to an effective 2-state model

Most commonly, diabatic models are applied as 2-state approaches[23-31, 33-44] and it was only recently that we showed that multi-state treatments are essential for the analysis of closed-shell reactions in terms of transferrable parameters.[52] However, a critical concept is the notion that the ground-state can be considered to have a "twin" state whose properties in an effective 2-state model are intricately linked to those of the ground state. This is an old concept[25-29] but previously the identity of the twin state was incorrectly assigned, and our contribution has been to determine just what it is.[52] For XH_3 inversion, the twin state is the double valence excitation D. While the inclusion of Rydberg states considerably complicates this scenario, the basic qualitative ideas remain sound. The simplest approach is to ignore the introduced perturbations and define an effective 2-state Hamiltonian in a localized-diabatic-state basis $\{L',R'\}$ as[52]

$$\mathbf{H'^{2L}} = \begin{bmatrix} T_2 + \frac{k}{2}(\tau + \sqrt{2}\tau_{m2})^2 & 2J_2 \\ 2J_2 & T_2 + \frac{k}{2}(\tau - \sqrt{2}\tau_{m2})^2 \end{bmatrix} \qquad (11)$$

where $T_2 = T - \dfrac{\lambda_2}{2} + J_G + J_2$ and

$$J_2 = \frac{J_G + J_D}{2},$$

$$\tau_{m2} = \frac{\tau_{mG} + \tau_{mD}}{2}, \text{ and} \qquad (12)$$

$$\lambda_2 = 2k\tau_{m2}^2.$$

If the ground-state surface is double welled then these parameters may be determined from simple properties of the adiabatic potential-energy surfaces obtained using electronic structure computation methods as

$$J_2 = \frac{\varepsilon_d(0) - \varepsilon_g(0)}{4},$$

$$\lambda_2 = \Delta E^{\ddagger} + |J_2| + \left[(\Delta E^{\ddagger})^2 + 4|J_2|\Delta E^{\ddagger} \right]^{1/2}, \text{ and} \qquad (13)$$

$$\tau_{m2} = \tau_e \left[1 - \left(\frac{2J_2}{\lambda_2} \right)^2 \right]^{-1/2}$$

where $\varepsilon_g(0)$ and $\varepsilon_d(0)$ are the values of the ground-state and doubly excited state energies at the planar D_{3h} geometry $\tau=0$, respectively, while $\Delta E^{\ddagger}$ and τ_e are the well depth and equilibrium geometry of the adiabatic ground-state, respectively.[52] If the diabatic potentials are harmonic then λ_2 is also unexpectedly but simply given as half of the vertical excitation energy at the adiabatic equilibrium bond angle, a quantity that can be readily accessible both computationally and spectroscopically.[52] Formulae revised to include the diagonal correction to the Born-Oppenheimer approximation are available[104] but the effects are negligible for the XH_3 series. Alternatively, for single-welled ground states, these parameters may be obtained as

$$J_2 = \frac{\varepsilon_d(0) - \varepsilon_g(0)}{4},$$

$$\frac{2J_2}{\lambda_2} = \frac{\dfrac{\partial^2 \varepsilon_d}{\partial \tau^2} - \dfrac{\partial^2 \varepsilon_g}{\partial \tau^2}}{\dfrac{\partial^2 \varepsilon_d}{\partial \tau^2} + \dfrac{\partial^2 \varepsilon_g}{\partial \tau^2}},$$

$$k_2 = \frac{1}{2} \left(\frac{\partial^2 \varepsilon_d}{\partial \tau^2} + \frac{\partial^2 \varepsilon_g}{\partial \tau^2} \right), \text{ and} \qquad (14)$$

$$\tau_{m2} = \left(\frac{\lambda_2}{2k_2} \right)^{1/2}.$$

What these equations tell is that, whilst the ground-state has a conical intersection seam with the singly excited state that is very important when it comes to understanding non-adiabatic chemical reactions, the global properties of the ground-state surface appear to be determined by a different seam, that between the ground-state and the doubly excited state. This occurs because of the presence of a real conical intersection seam between the singly excited state and the doubly excited state that also significantly influences the ground-state properties. So if one is studying non-adiabatic dynamics across the g-s conical intersection, then the physical parameters J_G, λ_G, τ_{mG}, etc. are relevant, but if the ground-state surface shape is being studied, the these quantities renormalized to $2J_2$, $2\lambda_2$, $2^{1/2}\tau_{m2}$, etc. are required instead. Only these later parameters allow properties of different chemical systems to be compared, e.g., electron-transfer reactions to XH_3 inversion to XH_3^+ inversion to benzene aromaticity to hydrogen bonding, etc..[52, 104-106]

d) Calculated ground-state adiabatic potential-energy surfaces and their relation to experiment.

Table 1 gives the properties of the ground-state adiabatic potential-energy surfaces for the XH_3 series evaluated using the CAS(2,2) (at MP2 geometries) and CCSD methods with, for CCSD, basis sets ranging from minimal to quadruple zeta. These are compared therein to available experimental data as well as to CCSD(T)/aug-cc-pwCVQZ values. Results for CCSD at the triple-zeta (TZP) level are accurate to 0.03-0.09 eV (0.7-2.1 kcal mol^{-1}) for the well depths $\Delta E^{\ddagger}$ for, in order, NH_3 to BiH_3. They are also accurate to within 1° in the HXH equilibrium bond angle θ_e for all molecules. This accuracy is sufficient for our purposes as the diabatic-model fits to the ground-state and excited-state surfaces (given also in the table) can only reproduce the original calculated data to about this accuracy. Higher-level calculations do achieve much greater accuracy,[107-113] however, and indeed in modern times are used in extensive diabatic models to fit entire ground-state potential-energy surfaces with high accuracy. The deduced model parameters may be twigged slightly to reproduce extensive observed spectroscopic data sets to generate "experimental" ground-state surfaces for NH_3,[57, 58] PH_3,[59] SbH_3,[60] and BiH_3.[61] At this level of accuracy, the diagonal correction to the Born-Oppenheimer approximation must be taken into account, but such treatment is not necessary herein.

e) Calculated vertical excitation energies including new assignments for the VUV absorption spectrum of NH_3.

In Table 2 are compared calculated and observed spectroscopic properties of NH_3. In total 7 vertical excitations are considered, those to the r ($n \rightarrow 3s$), dr ($n \rightarrow 3s, n \rightarrow 3s$), and s ($n \rightarrow \sigma^*_A$) states used in the diabatic model as well as for the valence excitations $n \rightarrow \sigma^*_E$, $\sigma_E \rightarrow \sigma^*_E$ (which has allowed transitions of both a' and e symmetry), and $\sigma_E \rightarrow \sigma^*_A$. The observed absorption of NH_3 has its first maximum at 6.5 eV corresponding to the Rydberg absorption r, leading to vertical ionization $n \rightarrow \infty$ at 10.9 eV.[63] Observed and calculated vertical ionization potentials for all of the XH_3 molecules are given in Table 3 and these, along with the energy of the r band, are reproduced quantitatively by the best calculations. In particular, the cc-pVDZ – cc-pVQZ basis sets are in error by only 1.2 – 0.6 eV for the energy of r, despite the absence of augmented functions in the basis set. This near-quantitative agreement is exploited throughout this work to allow easy description of the effects of the Rydberg transitions on the valence states.

Absorption at 16.3 eV and 25.3 eV is also observed to Rydberg bands leading up to the ionization potentials for $\sigma_E \rightarrow \infty$ and $\sigma_A \rightarrow \infty$ at 16.4 and 27.3 eV, respectively.[114] Two other broad bands are also observed centred at 18.4 eV and 31.5 eV, although originally only part of the 18.4 eV band was in the observable range and so this band was first assigned at 22 eV whilst the higher-energy band was observed partially resolved into components at 30 eV and 33 eV.[64] Both systems were attributed to double excitations, despite the typically low oscillator strength for such bands in one-photon spectroscopy.[64, 114]

PCCP

Physical Chemistry Chemical Physics

Dynamic Article Links ▶

ARTICLE TYPE

Table 1. Observed properties of XH₃ compared to calculated adiabatic potential-energy surface minima and those from various fits of the angular potential to a diabatic form containing # free parameters: R_{XH}- equilibrium XH bond length, τ_e- equilibrium torsion angle, θ_e- corresponding equilibrium HXH bond angle (Eqn. (1)), $\Delta E^{\ddagger}$ - activation energy for inversion.

XH₃	Method	Basis	#	R_{XH} / Å		τ_e / °			θ_e / °			$\Delta E^{\ddagger}$ / eV		
				Obs[a] [BC][f]	Calc	Obs[a] [BC][f]	Calc	Fit	Obs[a] [BC][f]	Calc	Fit	Obs[a] [BC][f]	Calc	Fit
NH₃	CAS(2,2)	STO-3G	8	1.016	1.055	21.4	25	25	107.5	104	104	0.220[b]	0.54	0.54
	CAS(2,5)	aSTO-3G	11	[1.010]	1.050	[22.0]	25	23	[106.8]	104	105	[0.231]	0.62	0.65
	CCSD	STO-3G	8		1.070		28	28		100	100		0.82	0.81
	CCSD	aSTO-3G	11		1.057		29	27		98	101		1.20	1.24
	CCSD	6-31G*	11		1.021		23	21		106	108		0.30	0.41
	CCSD	cc-pVDZ	11		1.026		25	23		104	105		0.37	0.39
	CCSD	cc-pVTZ	11		1.013		23	22		106	107		0.27	0.30
	CCSD	cc-pVQZ	11		1.010		22	23		107	106		0.24	0.24
PH₃	CCSD	STO-3G	11	1.420	1.412	32.9	34	33	93.3	92	93	1.38[ci]	2.90	2.92
	CCSD	cc-pVDZ	11	[1.412]	1.43	[32.5]	33	31	[93.9]	94	96	[1.440]	1.59	1.48
	CCSD	cc-pV(T+d)Z[g]	11		1.414		33	30		94	97		1.50	1.50
	CCSD	cc-pV(T+d)Z	11		1.414		33	29		94	99		1.50	1.49
AsH₃	CCSD	STO-3G	11	1.520	1.491	33.8	34	33	92.0	92	93	~1.38[ij]	2.42	2.44
	CCSD	cc-pVDZ-PP	11	[1.518]	1.526	[33.5]	34	33	[92.5]	92	93	[1.760]	1.93	1.88
	CCSD	cc-pVTZ-PP	11		1.518		34	32		93	95		1.82	1.78
SbH₃	CCSD	STO-3G	11	1.709	1.677	34.2	33	32	91.5	93	94	~1.63[di]	2.00	2.03
	CCSD	cc-pVDZ-PP	11	[1.711]	1.716	[33.7]	34	33	[92.2]	92	93	[1.916]	2.07	1.97
	CCSD	cc-pVTZ-PP	11		1.716		34	33		92	93		1.99	1.92
BiH₃	CCSD	cc-pVDZ-PP	11	1.788	1.804	35.1	35	35	90.3	91	91	~1.67[ei]	2.75	2.86
	CCSD	cc-pVTZ-PP	11	[1.797]	1.804	[34.8]	35	33	[90.7]	91	93	[2.549]	2.65	2.55

[a]: From Jerzembeck et al.;[115] [b]: From. Yurchenko et al.[57] and Huang et al.,[58] traditional Swalen and Ibers[103] value 0.25 eV; [c]: From Sousa-Silva et al.;[59] [d]: From Yurchenko et al.;[60] [e]: From Yurchenko et al.;[61] [f]: Best calcualtion we perform, CCSD(T)/aug-pwCVQZ but without Born-Oppenheimer breakdown or spin-orbit corrections. [g]: alternative assignemnt with *r* below *s*; [h]: alternatively[113] R_{NH} = 1.012 Å, τ_e = 22.1°, θ_e = 106.7°; [i]: rough approximation as experimental data only available up to ~ 0.5 eV in the torsional mode; [j]:From Costain and Sutherland.[116]

Table 2: Comparison of observed and calculated SAC-CI (very similar to EOM-CCSD)[81] ground-state vertical excitation energies for NH₃, in eV.

Basis	r	dr	s	$n \rightarrow \sigma^*_E$	$\sigma_E \rightarrow \sigma^*_E$ (a')	$\sigma_E \rightarrow \sigma^*_E$ (e)	$\sigma_E \rightarrow \sigma^*_{NH}$
STO-3G	-	-	14.6	16.0	28.7	25.1	22.2
cc-pVDZ	7.7	24.4	23.4	20.0	26.1	26.8	29.5
cc-pVTZ	7.3	23.8	18.6/19.7	20.5	27.6	26.3	24.7
cc-pVQZ	7.1	23.5	19.0/25.4	18.1	24.3/32.8	23.8/33.0	27.8
aug-cc-pVDZ	6.5	~28	25.4	21.4	27.5	27.9	30.8
d-aug-cc-pVDZ	6.5	~28	20.6/28.1	23.5/25.5		29.3	
aug-cc-pVTZ	6.5	28.1	16.2/26.7	16.4/23.7	23.6/30.1	22.3/28.7	21.8/31.7
Observed	6.5 [a]			18.4[b]		30 and 33, broad[b]	

[a]: From Robin[62]; [b]: From Ishikawa et al.[114].

ARTICLE TYPE

Table 3. Observed, calculated EOM-CCSD/VTZ and fitted vertical excitation energies to the valence (*s*), double valence (*d*), and Rydberg (*r*) states of XH₃ molecules, in eV, as well as the CCSD(T)/aug-cc-PVQZ calculated and observed vertical ionization potentials, in eV.

X	*s*		*d*		*r*		Vert. IP	
	Cal	Fit	Cal.	Fit	Cal	Fit	Cal	Obs[b]
N	18.6	18.4		43.4	7.3[a]	7.5	10.9	10.9
P	7.9[c]	8.0	19.9	20.2	14.1	13.2	10.6	10.6
As	7.7	7.6		19.7	13.2	12.4	10.5	10.5
Sb	7.4	7.1	18.4	18.2	11.3	10.8	9.8	10.0
Bi	7.3	6.6	16.1	15.7	11.9	11.1	10.0	

[a]: obs. 6.5 eV;[62] for convergent calculations using larger basis sets see Table 2. [b]: From Potts and Price;[63] [c]: Obs. 6.9 eV.[117, 118]

The 18.4 eV band was assigned to the *dr*-type series transitions *n*→3s,*n*→? leading up to an observed very weak ionization process at 24 eV involving *r* excitation plus ionization, *n*→3s,*n*→∞.[119] This would appear feasible as the isolated ionization process *n*→∞ occurs at 10.9 eV whilst the *r* absorption *n*→3s occurs at 6.5 eV, summing to 17.4 eV, amidst the observed band. However, the depression of the lowest Rydberg transition *n*→3s to 6.5 eV, 4.4 eV lower than the ionization continuum *n*→∞, occurs because of the strong interaction between the *r* and *s* states, and as a result the calculations always place the *dr* excitation *n*→3s,*n*→3s at *higher* energy than that of the full ionization *n*→3s,*n*→∞. Hence the calculations do not support the concept that significant absorption *n*→3s,*n*→? occurs at energies 6 eV less than the ionization potential of 24 eV. Also, the calculations do not suggest that the transition moment of this band could be sufficient to provide the observed absorption.

The broad bands observed in the 27-35 eV range with possible maxima at 30 and 33 eV are very intense, comparable with those of the strongest Rydberg transitions. All double excitations manifested in the calculations are very weak and could not be reasoned to account for the major part of the observed absorption.

Originally, the possibility that the unassigned absorption could be attributed to resonances associated with valence excitations was not considered. All calculations indicate that the *n*→σ*ₐ band *s* is very weak and therefore unlikely to be directly detected in the experiments. However, the σ_E→σ*_E system is predicted to yield a very strong in-plane (e) transition and a strong axial (a') transition comparable to the intensities of Rydberg bands, while σ_E→σ*ₐ is predicted to be of medium strength and *n*→σ*_E to be weak. Table 2 shows that *n*→σ*_E is predicted to lie near to the observed weak band at 18.4 eV, whilst the other bands are predicted in the vicinity of the intense absorption in the 26-20 eV region using valence basis sets. Adding augmented functions to these basis sets allows better representation of the Rydberg states but basis-set dependent resonances with the valence states are predicted, distributing the single-excitation intensity of the 22-33 eV range. While calculations in which the Rydberg and continuum orbitals are represented using say Green's functions (rather than the discrete representation used herein) are required for an authoritative assignment, it seems reasonable to reassign

the 18.4 eV band to the *n*→σ*_E resonance and the 30 eV and 33 eV systems to a σ_E→σ*_E and/or σ_E→σ*ₐ resonance combination.

Specifically, the *n*→σ*_E band is predicted to be at 16 eV by STO-3G, changing to 20, 21, and 18 eV as the valence basis set is increased from double to quad zeta. Adding a single set of augmented functions pushed the band up by 1 eV but adding a second set introduces an accidental resonance that splits the band into components of which the most obvious appear at quite high energy, 23.5 and 25.5 eV. Considering only the easily interpretable results, the calculations appear to support assignment of the observed 18.4 eV band to this resonance.

Concerning the development of diabatic models to understand the ground-state structure, Table 2 shows that the *dr* double excitation *n*→3s,*n*→3s occurs at ca. 4 times the energy of the single *r* excitation *n*→3s independent of basis set and is therefore a robust feature of the calculations. Similarly, the critical valence excitation *s* is robustly described. It is upon these properties that the diabatic model is based and conclusions concerning why NH₃ has a qualitatively different bond angle to the other series members are drawn. Tables 1 and 3 combine to show how the calculations reproduce other experimental data for the whole of the XH₃ series.

f) Potential-energy surfaces fitted with the 11-parameter 6-state diabatic model.

Table 4 gives the diabatic parameters fitted to a wide range of electronic structure calculations performed for the XH₃ series.
i. Properties of NH₃ evaluated using the STO-3G and aSTO-3G bases.

Fig. 2 shows the calculated and fitted surfaces for NH₃ obtained using small basis sets only. These small basis sets are the minimal STO-3G basis that allows for valence excitations only plus that augmented by a single N *s* function to crudely introduce the 3s Rydberg transition. Results are shown for both CASSCF and EOM-CCSD calculations. The EOM-CCSD calculations equally include all orbitals but preferentially treat the ground-state with respect to the single excitation and the single excitation with respect to the double excitation, whereas the CASSCF calculations treat each state equivalently but non-key orbitals are included inconsistently.

For the STO-3G basis only the simplest CASSCF calculation CAS(2,2) is needed, whereas CAS(2,5) is used for the aSTO-3G basis, including all unoccupied orbitals to allow for orbital switching as a function of geometry. An advantage of the CASSCF method is that only a limited number of excited states are manifested. The CAS(2,2) calculations produce only the key 3 valence states *g*, *s*, and *d*. However, the CAS(2,5) calculations deliver 7 states whereas only 6 (*g, s, d, r, rv, dr*) are anticipated. The additional state is the *n*→σ*_E,*n*→σ*_E double excitation and is easily identified and eliminated. However, identifying the nature of the other 6 states can be difficult as one must decide which order to place *s* and *r* (i.e., is the valence state lower or higher in energy than the 3*s* Rydberg state), with a follow-on problem for *d, rv,* and *dr*. We proceed by examining the form of the orbitals and the partitioning of the excited-state wavefunctions into contributions involving different orbital excitations. The σ*ₐ orbital is characterized by its valence antibonding nature whilst the Rydberg orbital is characterized by

PCCP

Physical Chemistry Chemical Physics

Dynamic Article Links ▶

ARTICLE TYPE

Table 4. Diabatic-model potentials containing # free parameters fitted to calculated ground and excited-state potential energy surfaces of XH_3 molecules.

XH_3	Method	Basis	#	J_G	J_D	α_G	α_D	k	γ_G	γ_D	k_4	E_R	Γ_R	V_{RV}
				eV	eV	meV/°	meV/°	meV/°²	meV/°³	meV/°³	μeV/°⁴	eV	eV	eV
NH_3	CAS(2,2)	STO-3G	8	6.09	7.64	0.264	0.343	7.61	-0.21	-0.36	-6.68	0	0	0
	CAS(2,5)	aSTO-3G	11	8.97	13.45	0.341	0.298	9.17	-0.26	0.12	-4.24	7.48	4.11	4.29
	EOM-CCSD	STO-3G	8	5.87	7.12	0.249	0.340	6.27	-0.09	0.02	13.38	0	0	0
	EOM-CCSD	aSTO-3G	11	7.27	15.12	0.286	0.407	6.45	-0.26	-1.42	-10.1	6.88	6.52	4.95
	EOM-CCSD	6-31G*	11	12.21	18.11	0.335	0.193	8.00	-0.31	-1.15	-12.56	10.85	3.71	8.3
	EOM-CCSD	cc-pVDZ	11	8.33	12.93	0.238	0.378	6.64	-0.17	-1.15	-11.59	10.73	6.50	7.26
	EOM-CCSD	cc-pVTZ	11	6.82	12.27	0.224	0.276	6.48	-0.14	-0.45	-6.74	9.08	7.77	4.92
	EOM-CCSD	cc-pVQZ	11	5.95	13.42	0.198	0.356	6.33	-0.19	-0.31	-8.70	11.89	1.44	5.70
PH_3	EOM-CCSD	STO-3G	8	3.43	4.78	0.273	0.365	8.18	0.03	-0.65	0.02	0	0	0
	EOM-CCSD	cc-pVDZ	11	4.29	3.91	0.269	0.177	8.44	-0.22	-0.08	-17.0	9.67	6.22	4.15
	EOM-CCSD	cc-pV(T+d)Z[a]	11	3.74	5.02	0.258	0.291	9.40	-0.22	-0.22	-19.95	7.47	0	2.57
	EOM-CCSD	cc-pV(T+d)Z	11	3.37	3.71	0.258	0.217	9.21	-0.22	-0.17	-20.2	7.98	2.89	2.38
AsH_3	EOM-CCSD	STO-3G	8	3.62	4.70	0.266	0.349	8.66	0.05	-0.55	-0.50	0	0	0
	EOM-CCSD	cc-pVDZ-PP	11	3.75	3.88	0.228	0.180	6.57	-0.13	0.12	-1.70	9.39	5.92	4.73
	EOM-CCSD	cc-pVTZ-PP	11	2.93	3.43	0.234	0.171	7.16	-0.17	0.12	-5.40	7.16	3.39	2.25
SbH_3	EOM-CCSD	STO-3G	8	3.12	3.97	0.237	0.328	9.04	0.12	-0.55	-0.62	0	0	0
	EOM-CCSD	cc-pVDZ-PP	11	2.89	3.39	0.208	0.190	7.09	-0.11	0.04	-5.19	8.49	3.79	4.36
	EOM-CCSD	cc-pVTZ-PP	11	1.98	3.14	0.195	0.170	6.65	-0.08	0.13	0.59	5.93	3.06	1.96
BiH_3	EOM-CCSD	cc-pVDZ-PP	11	2.74	2.96	0.187	0.185	4.63	0.02	-0.21	5.70	7.7	3.52	4.81
	EOM-CCSD	cc-pVTZ-PP	11	1.63	2.63	0.206	0.130	5.71	-0.18	0.05	-6.20	6.07	3.01	2.49

out-of-phase combinations of the Gaussians that dominate the N $2s$ and $3s$ orbitals, making identification straightforward.

All possible excited states made from single or double excitations of the CCSD reference are manifested in the EOM-CCSD calculations, and hence these intrinsically require more complex analysis. However, by noting the orbital compositions and excited-state descriptions in terms of orbital excitations and by following them adiabatically as a function of angle, identification of the states of interest can be accomplished. These states do undergo accidental resonances with other states and so the native properties of the excited states may in practice only be traced over restricted torsional bending amplitudes. As a result, the data points shown in Fig. 2 and later figures sometimes terminate only partly way along the potential-energy curves. This situation also arises during the CASSCF calculations except that the interfering states are not directly manifested. Sometimes the state of interest is clearly identifiable both before and after an avoided crossing and in such circumstances the actual data points in the avoided crossing region are replaced with values interpolated between the before and after regions to produce smooth surfaces for fitting.

Figure 2 shows the raw calculated surfaces (points) and their fit to the 8-parameter (STO-3G basis) or 11-parameter (aSTO-3G basis) models, revealing that the diabatic model accurately interpolates the calculated data. If the s and r states are incorrectly assigned, then poor quality fits usually emerge as the model treats valence and Rydberg states intrinsically differently. The most striking aspect of the figure is that the shown CASSCF and EOM-CCSD surfaces are in good qualitative agreement with each other, despite their considerable methodological and implementational differences. This indicates that the properties of ammonia inversion are realistically determined using traditionally conservative treatments of electron correlation.

The effects of inclusion of the Rydberg $3s$ orbital into the calculations are evidenced through the comparison of the STO-3G and aSTO-3G results in Fig. 2. The valence single s and double d excitation energies at the planar geometry are ca. 12 eV and 26 eV when only valence orbitals are included. Analysis indicates that the non-interacting diabatic Rydberg state R appears at near 7 eV (model parameter E_R, see Table 4) but interacts with the diabatic valence state S with a coupling of near 5 eV (model parameter V_{RV}). As the description used for the $3s$ orbital in terms of the STO-3G orbitals plus a single additional Gaussian function with an arbitrarily chosen exponent is crude, these results are not expected to provide a quantitative description of the Rydberg state. Rather, they just serve to indicate the fundamental physical situation in a simple and easy to interpret way. Significantly, S becomes considerably destabilized, resulting in two new adiabatic states at energies near 5 eV (r) and 18 eV (s). The double valence excitation d is destabilized proportionally more, going from ca. 26 eV using STO-3G to ca. 47 eV using aSTO-3G. These effects have a profound influence
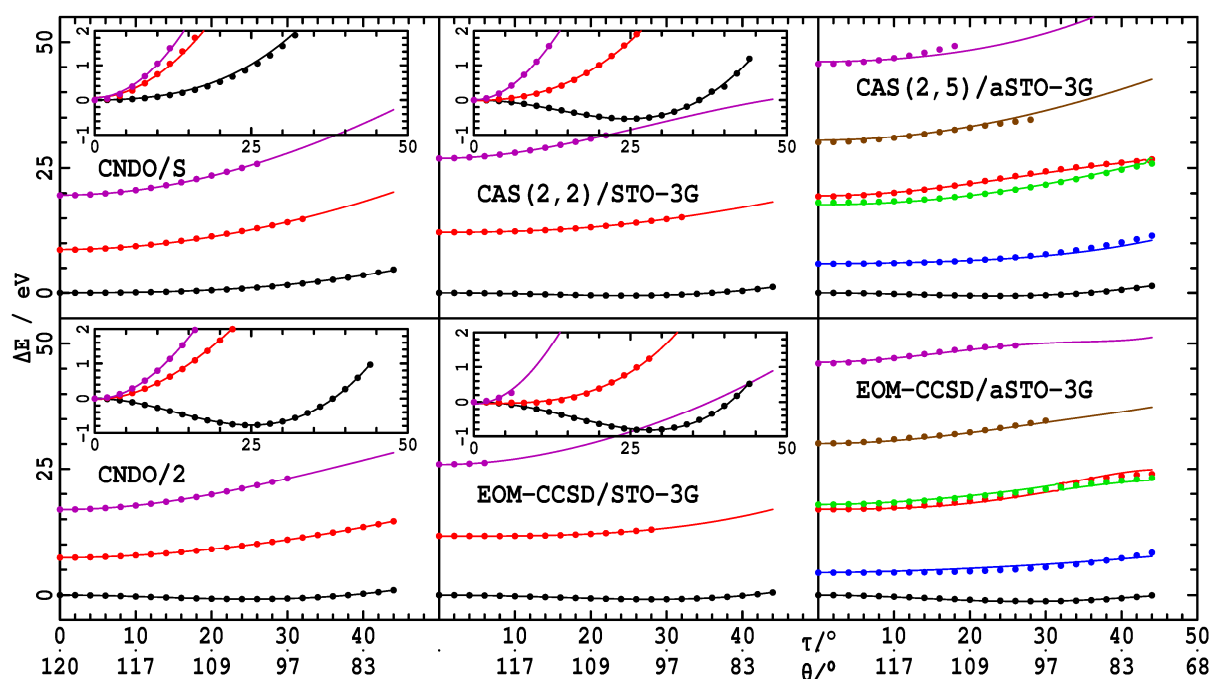
Fig. 2. Calculated adiabatic potential energy surfaces (points) and their fits using a diabatic model (lines) for the torsional potential of NH₃: black-ground state *g*, red- single valence excitation *s*, magenta- double valence excitation *d*, blue- single Rydberg excitation *r*, brown- Rydberg + valence double excitation *rv*, green- double Rydberg excitation *dr*. The inserts highlight the changes in energy vs. τ from those at the D$_{3h}$ structure.

on the inversion barrier especially from the EOM-CCSD calculations, increasing it from 0.81 eV to 1.24 eV (Table 1).

ii. Properties of NH₃ evaluated using large valence basis sets.

    While indeed the effect of adding a single 3*s* Rydberg orbital will turn out to be critical to understanding the nature of NH₃, the EOM-CCSD STO-3G and aSTO-3G well depths of 0.81 and 1.24 eV, respectively, are far removed from the observed value of 0.220 eV.[57, 58, 103] Figure 3 (and Tables 1 and 2) show how the EOM-CCSD ground and excited-state surfaces change as the basis set is increased from aSTO-3G to 6-31G* to cc-pVDZ to cc-pVTZ to cc-pVQZ. Identifying single orbitals and excited states as being either σ*$_A$ or N 3*s* character becomes difficult as many other orbitals interact to deform the orbital shapes. In

particular, the Rydberg orbital gains considerable H 2*s* character as well as valence σ$_A$ bonding character, whilst σ*$_A$ gains both N 3*s* and H 2*s* character.

    Overviewing the results in Table 4, we see that the energy E_R of the diabatic 3*s* Rydberg state *R* at the planar geometry is consistently near 11 eV, close to where these methods would predict the $2p \rightarrow 3s$ transition in the isolated nitrogen atom. However, the energy $2J_G$ of the diabatic valence state *S* decreases from 12 eV at the 6-31G* level to 8 eV at cc-pVDZ to 6 eV at cc-pVQZ, back to near its value for STO-3G. Indeed, 7 of the 8 valence-state diabatic parameters take on similar values for STO-3G and cc-pVQZ bases, indicating that the genera usefulness of STO-3G in describing valence-state properties and

Fig. 3. Calculated EOM-CCSD adiabatic potential energy surfaces (points) and their fits using a diabatic model (lines) for the torsional potential of NH₃: black- ground state *g*, red- single valence excitation *s*, magenta- double valence excitation *d*, blue- single Rydberg excitation *r*, brown- Rydberg + valence double excitation *rv*, green- double Rydberg excitation *dr*.
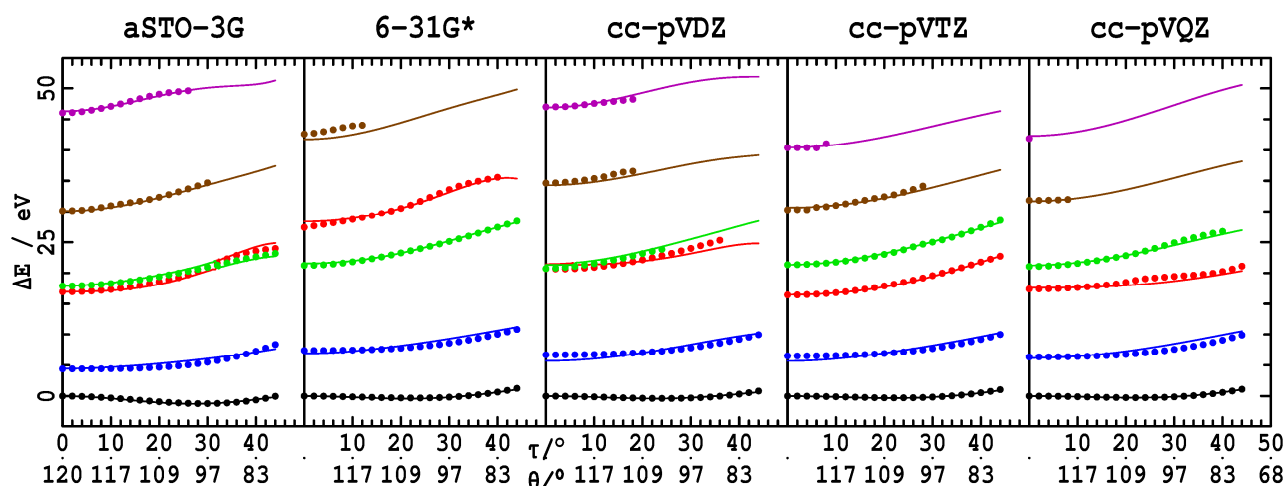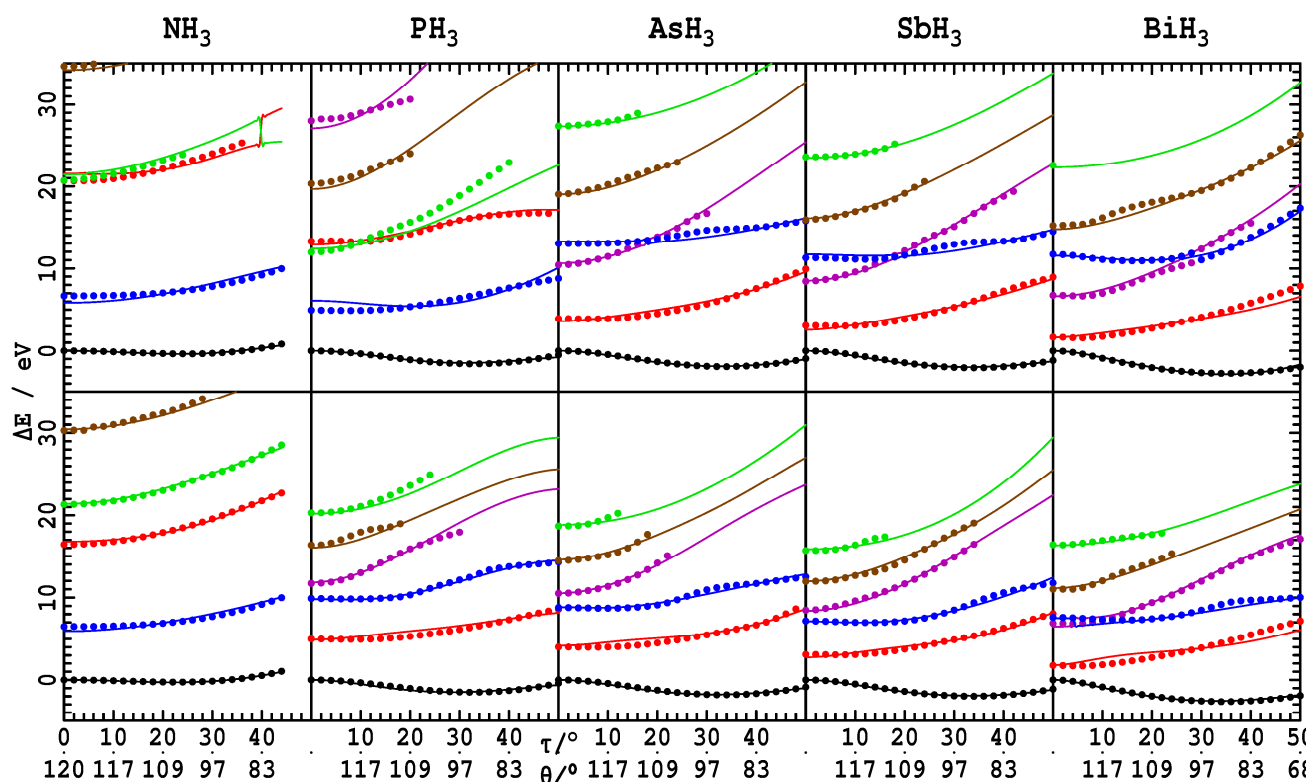
Fig. 4. Calculated EOM-CCSD adiabatic potential energy surfaces (points) and their fits using a diabatic model (lines) for the torsional potential of XH$_3$ molecules obtained using double-zeta bases (top row) and triple-zeta bases (bottom row): black- ground state *g*, red- single valence excitation *s*, magenta- double valence excitation *d*, blue- single Rydberg excitation *r*, brown- Rydberg + valence double excitation *rv*, green- double Rydberg excitation *dr*.

the need for a sophisticated treatment of the valence shell once Rydberg orbitals are introduced. However, one diabatic parameter, J_D, changes considerably from the STO-3G value once Rydberg orbitals are introduced, and this feature will in Section 4e become a focus for discussion.

iii. Properties of the XH$_3$ series evaluated using large valence basis sets.

Figure 4 compares the calculated and fitted adiabatic potential-energy surfaces for the XH$_3$ series obtained using EOM-CCSD with correlation-consistent basis sets at the double zeta (VDZ) and triple zeta (VTZ) levels. Examination of the wavefunctions indicates that the σ*$_A$ orbital clearly is lower in energy than the lowest-lying Rydberg orbital for AsH$_3$, becoming progressively more stable for SbH$_3$ and BiH$_3$. For these molecules, fitting the diabatic model assuming the diabatic orbitals are alternatively ordered leads to fits with mostly low errors but the extracted parameters change in unexpected ways. This effect is significant enough for it to be possible to determine that the orbital ordering has reversed in comparison to that in NH$_3$ *independent* of wavefunction analysis, demonstrating the robustness of the diabatic approach. However, for PH$_3$, neither wavefunction analysis nor diabatic fitting provide a decisive qualitative picture of the orbital ordering. The σ*$_A$ valence and 4*s* Rydberg orbitals are near degenerate in this molecule. Tables 1 and 4 present results fitted to energies calculated using the triple zeta basis assuming both possible orderings, leading to the conclusion that *S* is actually slightly lower in energy than *R*, and this is the result depicted in Fig. 4 and other places. Comparison of the XUV absorption bands of Ar, HCl, H$_2$S, PH$_3$, and SiH$_4$ in the gas-phase and solid has also led to the conclusion that, whilst strong mixing does occur for PH$_3$, the valence state is dominant for Ar, HCl,

H$_2$S, and PH$_3$ but the Rydberg state is dominant for SiH$_4$.[118, 120] Nevertheless, the lowest-energy observed VUV transition in PH$_3$ is often called the "Rydberg band".[117]

Overall, Table 1 shows that the HXH equilibrium bond angles from the fits are accurate to typically within 2° of the raw surface values for all heavy atoms but P for which errors grow to 5°. From this data, the variations found for the XH$_3$ series at the TZP level are displayed in Fig. 5a, highlighting the anomaly for PH$_3$. This anomaly arises as the *S* and *R* diabatic states are near degenerate, providing the worst-case scenario for the appropriateness of the diabatic Hamiltonian, Eqn. (10).

While even 2° differences are large on the scale to which angles and measured and discussed, the resulting differences to the potential-energy surfaces are small on the scale of the energies accessed by the 6 molecular potential-energy surfaces. Hence they are mostly not obvious looking at say Figs. 2-4. Always the equilibrium angle is fitted to be too large, however, suggesting that systematic improvement in the analysis is possible. The fitted well depths are accurate to typically 0.03 eV for NH$_3$ increasing to 0.1 eV for BiH$_3$. As highlighted in Fig. 5b, this parallels the actual changes in the barrier height which increases from 0.22 eV to 2.6 eV down the series. All optimized bond lengths R_{XH} at the adiabatic equilibrium geometry are close to the experimental and very high quality theoretical estimates (Table 1), and the vertical transition energies for key states at this geometry differ from the calculated values (Table 3) by on average just -0.4±0.4 eV.

f) Reliability of the diabatic-model parameters
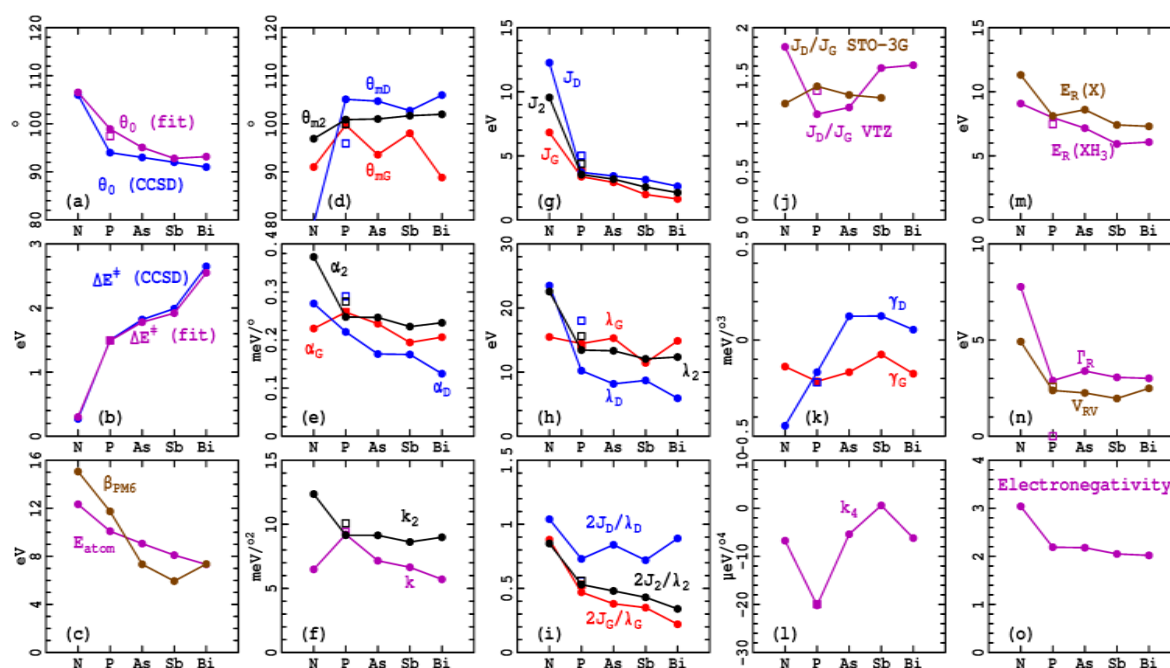
One measure of the success of the diabatic model is that the

Fig. 5. Variation of adiabatic and diabatic XH_3 properties, unless otherwise indicated evaluated using EOM-CCSD with triple-zeta bases, see text.

shapes of 6 potential energy surfaces are fitted using just 11 parameters. This is less than half the number of parameters required by a Taylor-series expansion involving just 0th, 2nd, and 4th order terms (later in Section 4d such Taylor expansions are
[5] also shown often to be very inaccurate). This indicates that the information contained in the diabatic-model equations reflects the factors controlling the molecular chemistry and spectroscopy. However, for the parameters to be robust and have an identifiable physical meaning, they must vary in a systematic and chemically
[10] sensible way as the basis set and heavy atom are varied. While both of these effects can be examined based on the data in Table 4, the effects of changing the heavy atom are highlighted in Fig. 5 which shows the variation between elements of the 11 diabatic-model parameters evaluated at the TZP level, properties derived
[15] from these parameters, related adiabatic properties, and other properties of interest.

The critical diabatic-model parameters J_G and J_D (Fig. 5g), α_G, and α_D (Fig. 5e), and k (Fig. 5f) show systematic variations and hence have clear physical meaning. Specifically, the force
[20] constant k changes little except for P for which the diabatic Hamiltonian is challenged owing to the near degeneracy of the diabatic σ^*_A and P $4s$ orbitals. Also, the resonance integrals J_G and J_D show marked differences between N and P-Bi and as a function of basis set, but these differences are attributed to actual
[25] chemical effects and basis set properties. Similarly, the Rydberg-state parameters E_R (Fig. 5m), V_{RV}, (Fig. 5n), and Γ_R (Fig. 5n) show systematic variations as a function of X, but they show more basis-set dependence that is desired. Figure 5m also compares the Rydberg-state energy in XH_3 to that calculated for
[30] atomic X using the same methods, showing similar variations (except for a small anomaly again owing to the orbital degeneracy in PH_3). This comparison demonstrates the reliability of the major fitted diabatic parameters. The remaining 3 parameters γ_G (Fig. 5k), γ_D (Fig. 5k), and k_4 (Fig. 5l) show larger
[35] variations with basis set and should be considered as being used primarily to empirically account for non-included effects in the

diabatic model, although γ_G may be meaningful.

While the vibronic coupling constants α_G and α_D are important quantities in their own right and can be evaluated analytically by
[40] codes such as MOLPRO[52] (and soon for TD-DFT in Q-CHEM),[121, 122] it is more usual to describe chemical and spectroscopic properties in terms of geometries and reorganization energies. For anharmonic diabatic potentials, these quantities are not uniquely defined and we choose their
[45] harmonic components τ_{mG}, τ_{mD}, λ_G, and λ_D defined in Eqns. (6) and (8). Alternatively, these quantities could be extracted from the actual properties of the diabatic surfaces $H_{L,L}^{3L}(\tau)$, $H_{C,C}^{3L}(\tau)$ and $H_{R,R}^{3L}(\tau)$ using Eqn. (5), or from the adiabatic equilibrium geometry. Table 5 and Fig. 5 present the deduced
[50] analytical values only, along with the implied values of the HXH diabatic-minimum bond angles θ_{mG} and θ_{mD} (Eqns. (1) and (6), Fig. 5d), reorganization energies λ_G, and λ_D (Eqn. (8), Fig. 5h), and the associated values of the control variables $2J_G/\lambda_G$ and $2J_D/\lambda_D$ (Fig. 5i). The best behaved quantity is found to be $2J_G/\lambda_G$
[55] but, while the other properties show more variation with basis set than was found for the model parameters themselves, the variations with X shown in Fig. 5 are better behaved. Provided also in Table 5 and Fig. 5 are the associated values of the corresponding parameters τ_{m2}, θ_{m2}, λ_2, etc. extracted using the
[60] effective 2-state model Eqn. (13). These are all well behaved and have properties similar to the state-dependent ones, with typically the 2-state model parameters sitting between the ones for the G and D interactions. This gives confidence that the parameters are meaningful. In particular, the perceived G-D differences and the
[65] aforementioned uncharacteristic large difference found for only NH_3 in the value of J_D between the STO-3G and cc-pVQZ bases reflect actual molecular and method properties.

Physical Chemistry Chemical Physics

ARTICLE TYPE

Table 5. Properties of XH₃ calculated adiabatic potential-energy surface minima and those from various fits of the torsional potential to a diabatic form containing # free parameters.

XH₃	Method	Basis	#	τ_m / °			θ_m / °			$J_2{}^a$ / eV	λ / eV			$2J/\lambda$		
				τ_{mG}	τ_{mD}	τ_{m2}	θ_{mD}	θ_{mD}	θ_{m2}		λ_G	λ_D	λ_2	$2J_G/\lambda_G$	$2J_D/\lambda_D$	$2J_2/\lambda_2$
NH₃	CAS(2,2)	STO-3G	8	35	45	27	91	75	101	6.9	18	31	18	0.67	0.49	0.76
	CAS(2,5)	aSTO-3G	11	37	31	28	87	94	99	11.2	25	19	28	0.71	1.39	0.79
	EOM-CCSD	STO-3G	8	40	54	28	84	61	100	6.5	20	37	19	0.59	0.39	0.70
	EOM-CCSD	aSTO-3G	11	44	63	30	77	46	97	11.2	25	51	31	0.57	0.59	0.72
	EOM-CCSD	6-31G*	11	42	24	32	80	104	94	15.2	28	9	35	0.87	3.89	0.87
	EOM-CCSD	cc-pVDZ	11	36	57	31	89	56	96	10.6	17	43	26	0.98	0.60	0.83
	EOM-CCSD	cc-pVTZ	11	35	43	30	91	79	97	9.6	15	24	23	0.88	1.04	0.85
	EOM-CCSD	cc-pVQZ	11	31	56	30	95	58	97	9.7	12	40	23	0.96	0.97	0.85
PH₃	EOM-CCSD	STO-3G	8	33	45	27	93	76	101	4.1	18	33	19	0.38	0.29	0.44
	EOM-CCSD	cc-pVDZ	11	32	21	28	95	108	100	4.1	17	8	15	0.50	1.05	0.54
	EOM-CCSD	cc-pV(T+d)Zᵇ	11	27	31	28	100	96	100	4.4	14	18	16	0.53	0.56	0.56
	EOM-CCSD	cc-pV(T+d)Z	11	28	24	27	100	105	101	3.5	14	10	13	0.47	0.73	0.53
AsH₃	EOM-CCSD	STO-3G	8	31	40	27	96	83	101	4.2	16	28	18	0.44	0.33	0.47
	EOM-CCSD	cc-pVDZ-PP	11	35	27	27	91	101	101	3.8	16	10	15	0.47	0.79	0.50
	EOM-CCSD	cc-pVTZ-PP	11	33	24	27	94	105	101	3.2	15	8	13	0.38	0.84	0.48
SbH₃	EOM-CCSD	STO-3G	8	26	36	27	102	89	101	3.6	12	24	15	0.50	0.33	0.48
	EOM-CCSD	cc-pVDZ-PP	11	29	27	27	98	101	101	3.1	12	10	14	0.47	0.67	0.45
	EOM-CCSD	cc-pVTZ-PP	11	29	26	26	98	103	102	2.6	11	9	12	0.35	0.72	0.43
BiH₃	EOM-CCSD	cc-pVDZ-PP	11	40	40	27	82	83	101	2.9	15	15	15	0.36	0.40	0.39
	EOM-CCSD	cc-pVTZ-PP	11	36	23	26	89	106	102	2.1	15	6	12	0.22	0.89	0.34

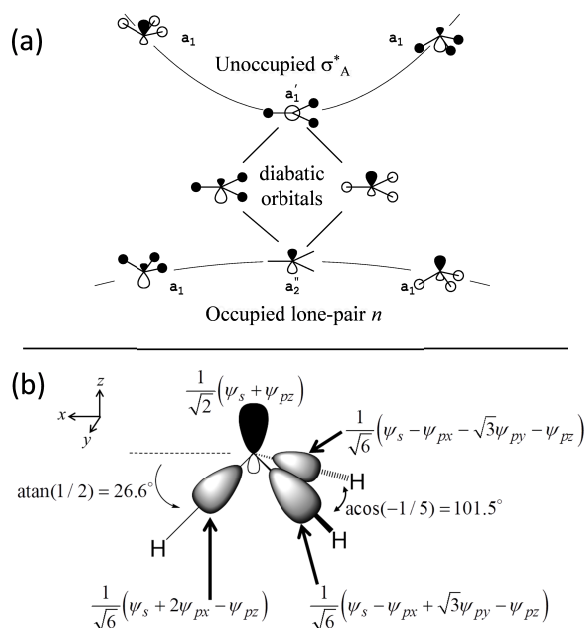ᵃ: J_G and J_D are given in Table 1, $J_2 \approx (J_G + J_D)/2$. ᵇ: alternative assignemnt with *r* below *s*.

4. Discussion

a) Orbital following

Pauling's concept of hybridization significantly influenced chemical understanding, pointing out that the shapes of molecules and the shapes of the bonding orbitals are intricately connected.[123, 124] This is expressed clearly in the *orbital following*[69] principle. For this principle to be used as a predictive tool for molecular structure rather than just an interpretive one, some mechanism is needed for determining the orbital shapes beforehand. The diabatic model provides such a method. At any particular angle, resonance mixes two geometry-independent diabatic orbitals to produce a lone-pair orbital of determined shape. Application of the orbital orthogonality condition is then sufficient to determine the shapes of the bonding orbitals. If the orbital following principle holds, then the orbital angles will match the bond angles.

Figure 6 shows how this works in practice. First, Fig. 6a contains a modified Walsh diagram[53, 54] indicating how the lone-pair *n* and antibonding σ*_A orbitals change as structures are distorted from planarity. The diabatic orbitals are given simply as the ± linear combinations of these orbitals at the planar structure, the contribution of which from the central X atom is of the form of *sp* hybrids $2^{-1/2}(\psi_s \pm \psi_{pz})$.[52] At the planar geometry the diabatic orbitals are degenerate and so the adiabatic orbitals result from full resonance between the diabatic orbitals. As the molecule distorts, this resonance is broken and the adiabatic orbitals slowly transform to be more like the *sp* diabatic ones. Figure 6b shows how bonding hybrid orbitals are constructed for the special case in which there is no resonance interaction at all. In this case the adiabatic lone-pair orbital becomes simply one of the *sp* diabatic orbitals. The hybrid orbitals thus produced have $s^{1/2}p^{5/2}$ character and are oriented at a torsional angle of $\tau = \text{atan}(1/2) = 26.6°$, making the HXH bond angle $\theta = \text{acos}(-1/5) = 101.5°$ (Eqn. (1)).

(a)

Unoccupied σ^*_A

diabatic orbitals

Occupied lone-pair n

(b)

$\dfrac{1}{\sqrt{2}}\left(\psi_s + \psi_{pz}\right)$

$\dfrac{1}{\sqrt{6}}\left(\psi_s - \psi_{px} - \sqrt{3}\psi_{py} - \psi_{pz}\right)$

$\text{atan}(1/2) = 26.6°$

$\text{acos}(-1/5) = 101.5°$

$\dfrac{1}{\sqrt{6}}\left(\psi_s + 2\psi_{px} - \psi_{pz}\right)$

$\dfrac{1}{\sqrt{6}}\left(\psi_s - \psi_{px} + \sqrt{3}\psi_{py} - \psi_{pz}\right)$

Fig. 6. (a) Modified Walsh diagram showing how sp hybridized diabatic orbitals on X interfere to produce pure p and s adiabatic orbitals at the planar geometry, and how the adiabatic orbitals decouple as XH$_3$ molecules distort. (b) An X sp diabatic lone-pair orbital $2^{-1/2}\left(\psi_s + \psi_{pz}\right)$ and its 3 orthogonal $s^{1/2}p^{5/2}$ bondable hybrid orbitals at a torsional angle of $\tau = 26.6°$ and HXH bond angle $\theta = 101.5°$.

A key feature of this analysis is that it predicts the orbital orientations to be the same for both XH$_3$ molecules and XH$_3^+$ radical cations, so that the orbital following principle would then predict the same geometries for both species, neglecting the small changes that occur to orbital properties upon molecular ionization. This is because the key properties in the diabatic model are one-electron properties such as resonance energies and vibronic coupling constants. Yet the geometries of these species are known experimentally to be very different and the diabatic model simply anticipates this through the renormalization of the diabatic bond-angle apparent in Eqn. (11) – the torsional angle $2^{1/2}$ times large for XH$_3$ than for XH$_3^+$ if the basic orbital properties are conserved. This change occurs owing to the electron occupation of the lone-pair orbital: the single electron present in XH$_3^+$ leads to a 2-state diabatic problem dominated by a single conical intersection seam whilst the double occupancy in XH$_3$ leads to 3 coupled diabatic states with 3 associated coupled conical-intersection seams.

Figure 7 shows how the angle between the bonding hybrid orbitals changes as a function of the HXH bond angle using simple 3-parameter diabatic models for NH$_3$, NH$_3^+$, BiH$_3$, and BiH$_3^+$. According to the orbital following principle, these two angles should always be equal. However, we see there are large deviations, with the angles between the bonding orbitals tending to the limit of $\theta = \text{acos}(-1/5) = 101.5°$ depicted in Fig. 6b for diabatic orbitals in the absence of resonance. This angle comes from a torsional angle of $\tau = \text{atan}(1/2) = 26.6°$ (Fig. 6b). Therefore the orbital following argument most directly applies only to the one-electron situation of the XH$_3^+$ series. Renormalization of the parameters for XH$_3$ changes these angles to $\tau = 2^{1/2}\text{atan}(1/2) = 37.6°$ and $\theta = \text{acos}[3\sin^2(2^{1/2}\text{atan}(1/2))/2-1/2] = 86.7°$. These critical values are listed in Table 6 and are the expected equilibrium angles in the absence of resonance coupling. Figure 7 shows that the Bi hydrides approach the uncoupled limit much faster than the N hydrides owing to their smaller value of $2J_2/\lambda_2$. These results are qualitatively consistent

with our high-level calculations. For NH$_3$, the angles between the natural hybrid orbitals have previously been calculated[125] and the results are shown in Fig. 7. These are in realistic agreement with the simple predictions of the 3-parameter diabatic model.

The orbital following theory was developed to explain equilibrium structures whereas Fig. 7 examines properties at arbitrary bond angles. It is interesting to note that at the equilibrium geometries of NH$_3$ (108°) and BH$_3$ (90°), the hybrid angles from the diabatic theory are within 2° of the bond angles, in accordance with basic expectations. Indeed, the assumption that orbital following controlled the equilibrium angle in the absence of resonance expounded in Fig. 6b is used to construct Fig. 7, making for a consistent analysis.
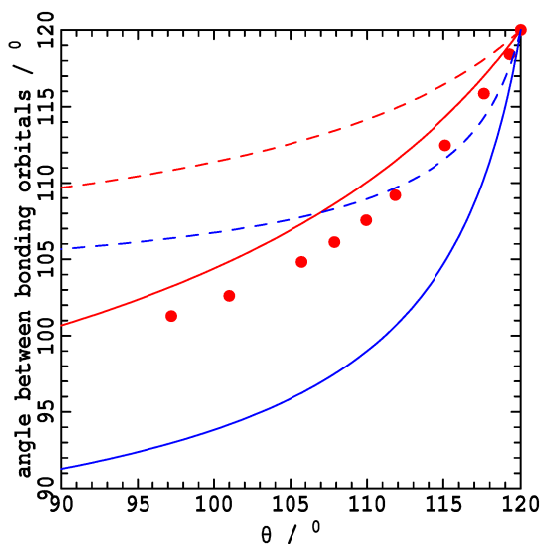
Fig. 7. The angle between the natural hybrid bonding orbitals, determined assuming that they are orthogonal to the lone-pair orbital composition determined from the 3-parameter diabatic model, as a function of the HXH bond angle. Red- X=N NH$_3$ ($2J_2/\lambda_2 = 0.79$, $\theta_{m2}=86.7°$), blue- X=Bi ($2J_u/\lambda_u = 0.38$, $\theta_{m2}=86.7°$), solid lines- for XH$_3$, dashed lines- for XH$_3^+$ (n.b., using XH$_3$ parameters), points- calculated values[125] for NH$_3$.

Table 6. Maximum orbital overlap predictions for the equilibrium bond angles in the absence of resonance ($J_G = J_D = 0$).

Molecule	Angle	Equation	Value
XH$_3^+$	τ_e	$\text{atan}(1/2)$	26.6°
	θ_e	$\text{asin}(-1/5)$	101.5°
XH$_3$	τ_e	$2^{1/2}\text{atan}(1/2)$	37.6°
	θ_e	$\text{acos}[3\sin^2(2^{1/2}\text{atan}(1/2))/2-1/2]$	86.7°

b) τ_{m2} and θ_{m2} as universal constants

The orbital following arguments lead to the conclusion that the equilibrium bond angles in the absence of resonance are specified as in Table 6. These results can be summarized as indicating that $\tau_{m2} = \text{atan}(1/2) = 26.6°$ and $\theta_{m2} = \text{acos}(-1/5) = 101.5°$ are expected to be universal constants, independent of composition X, ionization, calculation type, and basis set. Indeed, the deduced values of θ_{m2} for all 12 fits to XH$_3$ molecules reported in Table 5 for X $\neq$ N are between 100°-102°, independent of basis set and composition, averaging 101.1±0.5°. For NH$_3$, the same result holds for the STO-3G basis but the addition of the N 3s Rydberg orbital perturbs the picture, with the larger basis sets yielding 97°. Nevertheless, the magnitude of this anomaly is small and significant understanding of even NH$_3$ can be obtained assuming that universality holds. However, focusing on this discrepancy,

we see that whilst for P-Bi the influence of the Rydberg states can be accounted for simply by the extended diabatic model, the effects for N are more profound and act to change slightly the fundamental nature of the valence orbitals.

In Section 4g the properties of XH_3^+ are considered from a quantitative perspective. Preliminarily, we note that the CCSD(T)/aug-pwCVQZ calculated equilibrium bond angles are 120°, 113°, 112°, 112°, and 109° for NH_3^+ - BiH_3^+, respectively. These naively appear to be consistent with the expected asymptotic limit of the universal angle of = 101.5°.

The expectation that θ_{m2} is a universal constant arises as this parameter most directly affects the ground-state equilibrium geometry. At a crude level of approximation, ignoring the orbital dependence of the on-site repulsion between electron pairs, etc., one expects $\theta_{mG} = \theta_{mD} = \theta_{m2}$ and hence it is of interest to see if θ_{mG} and θ_{mD} also appear as universal constants. Table 5 shows this not to be the case, however, as θ_{mG} and θ_{mD} show fluctuations that there average (nb., Eqn. (12)) θ_{m2} does not. While part of these fluctuations arises from the difficulty of robustly fitting the parameters, part is also systematic. θ_{m2} is concerned mostly with the properties of the ground-state g and its "twin state" d,[52] the other parameters are controlled in addition by the properties of the single excitation s, the state that directly interacts with the key Rydberg state r. Even at the STO-3G level, θ_{mG} and θ_{mD} are differentiated, however, with θ_{mG} becoming the largest of the pair. When the energy of the diabatic Rydberg state R is lower than that for the diabatic valence state S (in Table 5 this is for X=N and for the X=P alternate assignment), this difference is enhanced, but when the valence state is the lowest then this difference is reversed.

Table 7. Parameters from the effective two-state model fit to semi-empirical potential energy surfaces for XH_3 molecules evaluated using CAS(2,2).

XH_3	Method	J_2 / eV	λ_2 / eV	$2J_2/\lambda_2$	τ_{m2} / °	θ_{m2} / °
NH_3	CNDO/S	4.9	8.9	1.09	20	99
PH_3	INDO/S	2.9	7	0.84	24	91
NH_3	CNDO/2	4.2	13	0.65	23	94
PH_3	CNDO/2	2.8	10	0.55	22	96
AsH_3	CNDO/2	2.4	10	0.49	23	94

Finally, we consider the predictions of simple but intuitive semi-empirical molecular-orbital methods such as CNDO/S, INDO/S, and CNDO/2. Historically, results from such calculations provided the first glimpses into quantitative understanding of molecular properties and aided in producing much of the chemical intuition that we inherit today. Fitted model parameters for XH_3 series members are given in Table 7 and show larger deviations from the universal angle $\theta_m = 101.5°$ than do the ab initio ones. This is at first surprising as simpler computational methods often neglect the subtleties that cause reality to differ from simplistic predictions. However, these methods also suffer from the well-known problem that different parameters must be used to describe ground-state geometries and reactivity (the "/2" parameterizations) than are used to describe spectroscopy (the "/S" parameterizations). Figure 2 demonstrates this property, showing that the CNDO/2 ground-state surfaces closely parallel the ab initio ones whilst CNDO/S predicts NH_3 to be planar ($2J_2/\lambda_2 = 1.09$). The diabatic analysis makes the primary cause

for these phenomena clear: explicit inclusion of the key Rydberg orbital is required for a fully robust semi-empirical theory. These method fail here not because they omit subtle effects but rather because their nature does not allow them to simultaneously describe spectroscopy and structure and hence they are fundamentally incapable of recognizing the importance of the universal angle.

c) The critical importance of $2J_2/\lambda_2$ in linking molecular structure to molecular spectroscopy

That θ_{m2} (or equivalently τ_{m2}) is a universal parameter means that at the simplest level only two parameters, say J_2 and λ_2, control the ground-state and twin-state properties calculated for each molecule by each computation method. However, the critical ratio $2J_2/\lambda_2$ controls many of these properties including the location of the XH_3 adiabatic ground-state minimum which from Eqn. (11) and standard 2-state diabatic relationship is[52, 126]

$$\tau_e = \sqrt{2}\tau_{m2}\left[1 - \left(\frac{2J_2}{\lambda_2}\right)^2\right]^{1/2}. \quad (15)$$

Hence now in the effective two-state diabatic description just *one* adjustable quantity controls the equilibrium bond angle.

As an initial evaluation of the usefulness of this result, we predict τ_e from the TZP values of $2J_2/\lambda_2$ listed in Table 5 (see also Fig. 5i). This ratio decreases dramatically between NH_3 and PH_3 (0.85 to 0.53) but then decreases slowly through AsH_3, SbH_3, and BiH_3 (0.48, 0.43, and 0.34). From Eqn. (15), the anticipated equilibrium bond angle θ_e therefore changes from 109° to 95° to 93° to 92° to 90° for NH_3 to BiH_3, paralleling the observed (Table 1) values of 108°, 93°, 92°, 92°, and 90°, respectively. This portrays a deep relationship connecting the ground-state equilibrium angle and well depth with the vertical excitation energy to the doubly excited twin state d at the planar geometry.

d) Predicting spectroscopic transition energies knowing just the ground-state equilibrium torsion angle and well depth.

To exploit the simplicity of the effective two-state diabatic model with only two free parameters, Eqn. (15) can be rearranged to determine the critical ratio $2J_2/\lambda_2$ knowing *only* the observed or calculated equilibrium bond angle τ_e:

$$\frac{2J_2}{\lambda_2} \approx \frac{2J_u}{\lambda_u} = \pm\left[1 - \frac{1}{2}\left(\frac{\tau_e}{\tau_{m2}}\right)^2\right]^{1/2}. \quad (16)$$

From this, the vertical transition energies to the d state at the planar and equilibrium geometries can immediately be obtained if the observed or calculated ground-state well depth $\Delta E^{\ddagger}$ is known[52]

$$\varepsilon_d(0) - \varepsilon_g(0) = 4|J_u| = 4\Delta E^{\ddagger}\left(\frac{2|J_u|}{\lambda_u}\right)\left(1 - \frac{2|J_u|}{\lambda_u}\right)^{-2}$$

$$\varepsilon_d(\tau_e) - \varepsilon_g(\tau_e) = 2\lambda_u = 4\Delta E^{\ddagger}\left(1 - \frac{2|J_u|}{\lambda_u}\right)^{-2}. \quad (17)$$

Table 8 shows results for $2J_u/\lambda_u$, J_u and λ_u evaluated using for τ_e and $\Delta E^{\ddagger}$ values taken (i) from experimentally refined surfaces for NH_3,[57] PH_3,[59] and $SbH3$[60] or else, for BiH_3, high-level full-dimensional potential-energy surfaces, (ii) from CCSD(T)/aug-cc-pwCVQZ calculations, and (iii) the analogous calculated quantities $2J_2/\lambda_2$ and $4J_2$ from Table 5 evaluated using actual excited-state energies from EOM-CCSD/VTZ calculations using Eqn. (13). The three sets of $2J/\lambda$ values are in good

ARTICLE TYPE

Table 8. Estimates of $2J_u/\lambda_u$ and the related energy of the double excitation twin state d at the planar geometry, $4J_u$, and at the ground-state equilibrium geometry, $2\lambda_u$, based on either observed, CCSD(T)/aug-cc-pwCVQZ, or CCSD/VTZ calculated ground-state equilibrium bond angles τ_e and inversion barrier heights $\Delta E^{\ddagger}$ taken from Table 1, obtained assuming the universality of $\theta_{m2} = \text{acos}(-1/5) = 101.5°$ (Eqns. (16)-(17)); the EOM-CCSD/VTZ multi-state calculated values of $2J_2/\lambda_2$ and $4J_2$ evaluated without this assumption from Table 5 are also provided for comparison.

XH$_3$	Observed					CCSD(T)/aug-cc-pwCVQZ					EOM-CCSD/VTZ							
	τ_e / °	$\Delta E^{\ddagger}$ eV	$2J_u/\lambda_u$	$4J_u$ eV	$2\lambda_u$ eV	τ_e °	$\Delta E^{\ddagger}$ eV	$2J_u/\lambda_u$	$4J_u$ eV	$2\lambda_u$ eV	τ_e °	$\Delta E^{\ddagger}$ eV	$2J_u/\lambda_u$	$4J_u$ eV	$2\lambda_u$ eV	$2J_2/\lambda_2$	$4J_2$ eV	$2\lambda_2$ eV
NH$_3$	21.4	0.22	0.82	23[a]	28[a]	22.0	0.23	0.81	21[a]	24[a]	22.8	0.27	0.79	20.4[a]	26[a]	0.85	38	45
PH$_3$	32.9	1.38[b]	0.48	10[b]	21[b]	32.5	1.44	0.50	12	20	32.5	1.5	0.50	12.1	24	0.53	14	27
AsH$_3$	33.8	1.38[b]	0.44	8[b]	17[b]	33.5	1.76	0.45	11	19	33.5	1.82	0.45	11.0	24	0.48	13	26
SbH$_3$	34.2	1.63[b]	0.41	8[b]	19[b]	33.7	1.92	0.44	11	16	33.8	1.99	0.44	10.9	25	0.43	10	24
BiH$_3$	35.1	1.67[b]	0.36	6[b]	16[b]	34.8	2.55	0.38	10	29	34.7	2.65	0.38	10.7	28	0.34	9	25

[a]: large errors arise from valence/Rydberg orbital inversion modifying τ_m combined with the instability of Eqn. (17) as of $2J_u/\lambda_u \to 1$.

[b]: $\Delta E^{\ddagger}$ extrapolated from observed transitions and/or calculated data only up to 0.5 eV.

agreement with each other, although the differences are largest for NH$_3$: 0.82 from Eqn. (15) using observed data, 0.79 from this equation using CCSD/VTD data, and 0.85 from the more general Eqn. (13). However, reasonable agreement for the spectroscopic transition energies is only found for PH$_3$ to BiH$_3$. For example, the predicted vertical excitation energies for NH$_3$ are 28 eV from Eqn. (17) using experimental data, 24 – 26 eV using calculated data, and 45 eV from the actual EOM-CCSD calculations. This problem arises as Eqn. (17) becomes unstable as $2J_u/\lambda_u \to 1$, producing large errors in the transition energy from small ones in $2J_u/\lambda_u$. Hence in practice this method is only useful for estimating excited-state energies when the lone pair is strongly localized on one side of the heavy atom.

e) Predicting the ground-state torsional potential energy surface knowing just the ground-state equilibrium torsion angle and well depth.

Figure 8 shows the torsional potentials from the experimentally refined (for NH$_3$,[57] PH$_3$,[59] and SbH$_3$[60]) or, for BiH$_3$, high-level full-dimensional potential-energy surfaces. These are compared to CCSD(T)/aug-cc-pwCVQZ surfaces and are in excellent agreement for the low-energy region to which the experimental surfaces were fitted. The CCSD(T)/aug-cc-pwCVQZ surfaces are fitted using: a 3-paramater diabatic model with τ_{m2} variable (unbroken lines), a 2-parameter diabatic model with $\tau_{m2} = \text{atan}(1/2) = 26.6°$ (short-dashed lines), and a two-parameter fit as quartic polynomials (long-dashed lines). The 3-parameter fits provide excellent descriptions of the torsional potentials, often with RMS errors less than 1 meV, but the fitted parameters have no obvious physical meaning.[52] However, the 2-parameter model fits lead to realistic predictions of excitation energies, as discussed earlier, and for most molecules provide excellent fits of the potentials out to large torsional angles. In contrast, 2-parameter fits using a quartic Taylor-expansion function produce very poor approximations to the vibration frequencies and well shape, particularly for small $2J_2/\lambda_2$. These results show that assuming the universal diabatic angle leads to simple and accurate methods for predicting the ground-state surface knowing only the equilibrium torsional angle and well depth.
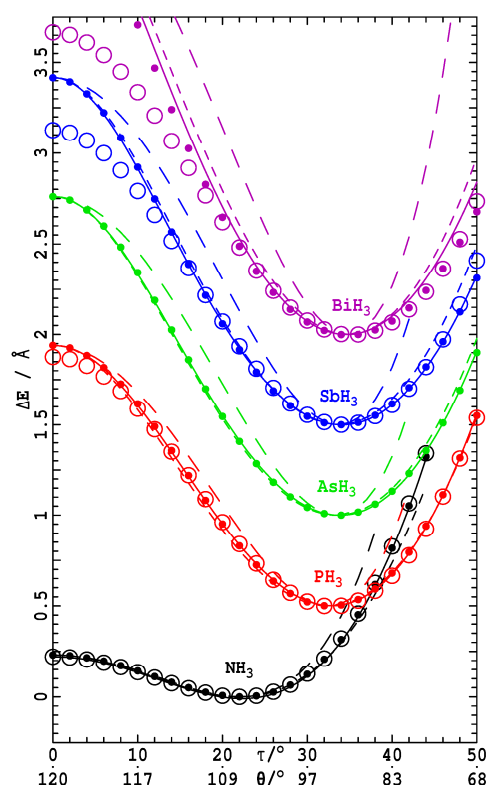
Fig. 8. Offset CCSD(T)/aug-pwCVQZ(-PP) torsional potentials for the XH$_3$ series (solid circles) are compared to results from full-dimensional surfaces (open circles) for BiH$_3$ and those as refined to fit experimental data for NH$_3$, PH$_3$, and SbH$_3$, and fitted by 3-parameter (solid lines), two-parameter (assuming $\theta_{m2} = \text{atan}(-1/5) = 101.6°$) (short-dashed line) models as well as quartic potentials (long-dashed lines). Note that only observed torsional levels up to ca. 0.5 eV in energy above the minima were available for inclusion in the surface refinements.

f) Why NH$_3$ is so different to PH$_3$ – BiH$_3$.

Figures 5g and 5h show that the sharp change in $2J_2/\lambda_2$ found between NH$_3$ and PH$_3$ comes from similar sharp changes in the individual properties $2J_2$ and λ_2, except that the change for λ_2 is smaller than that for $2J_2$. Both originate from the properties of the diabatic *sp* orbitals: the resonance integrals scale like

$$2J_2 = \langle \psi_s + \psi_p | H | \psi_s - \psi_p \rangle \qquad (18)$$

where ψ_s and ψ_p are the wavefunctions for the X orbitals, whilst λ_2 tells the energy of swapping one of the linear combinations for the other with the hydrogens placed at the diabatic angle τ_{m2}. Naively, one could expect the resonance energy to scale like the one-electron integrals, a simple indication of which is given by the atomic parameter β used in semi-empirical theories, and the values developed for PM6[127] for N-Bi are indicated in Fig. 5c. Similarly, the reorganization energy could be expected to scale with bond energies as swapping over the diabatic orbitals breaks chemical bonds, and so the CCSD/VTZ-calculated atomization energies E_{atom} are also shown in Fig. 5c. However, neither quantity mimics the behaviour of J_2 or λ_2. A quantity that does behave similarly is the atomic Pauling electronegativities and these are shown in Fig. 5o. It is difficult to establish a connection, however, as the electronegativities introduce only small changes whereas J_2 and λ_2 change markedly. More formally, the full list of contributions to J_2 at the CAS(2,2) level evaluated at the planar geometry can be expressed in terms of standard integrals from Hartree-Fock theory. This lists one-electron integrals and many two-electron integrals, one of which is the difference in the on-site repulsion integral (often called the "Hubbard U") for two electrons in the n orbital and for two electrons in the σ^*_A orbital. We focus on this contribution.

Figure 9 shows orbital isodensity surfaces determined using HYPERCHEM[128] for the σ^*_A orbitals of NH$_3$ and AsH$_3$ at their planar geometry evaluated using the STO-3G and aSTO-3G bases (to which 6-31G* results are very similar). For NH$_3$, the antibonding orbital has much hydrogen character and the orbital is spatially extended. The hydrogen orbitals interact with the Rydberg orbital in an *antibonding* way for NH$_3$ and in a *bonding* way for AsH$_3$. This fundamental change occurs owing to the reversed orbital ordering:
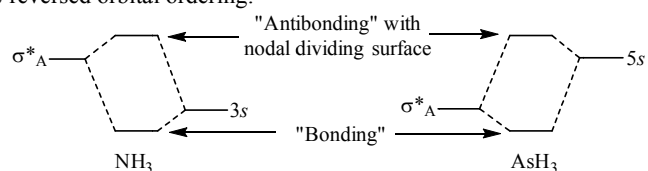
The antibonding combination found for NH$_3$ introduces a nodal surface between the hydrogens and the outer Rydberg shell, the effect of which is very apparent in Fig. 8: Rydbergization of the σ^*_A orbital in NH$_3$ compresses the electron density into a tight volume which has a profound effect on the orbital energy. Placing two electrons into this compressed orbital therefore develops a large electron-electron repulsion. It is this repulsion that becomes manifest in the large value of the resonance integral J_2 for NH$_3$. However, when the valence orbital is lower than the Rydberg orbital, the valence-dominated linear combination has bonding character, stabilizing the σ^*_A orbital to reduce the resonance energy. As Fig. 8 shows, this effect on the large AsH$_3$ molecular orbital is small, so it is really the Rydbergization-driven orbital compression of NH$_3$ that provides for its unusually large HXH bond angle of 108°.

Further evidence supporting this hypothesis comes from
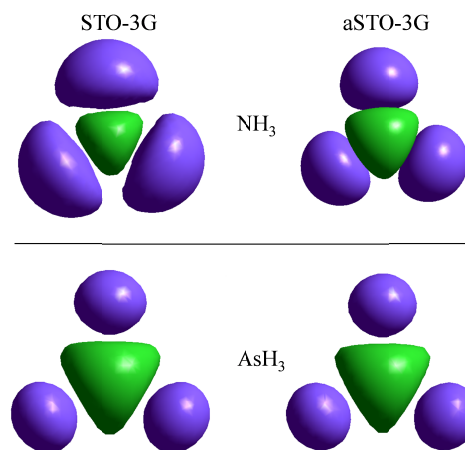
Fig. 9. Isodensity surfaces of the unoccupied σ^*_A valence orbital of NH$_3$ and AsH$_3$ that controls hybridization, at its planar D$_{3h}$ structure, evaluated using the Hartree-Fock method.

looking at the J_D/J_G ratio shown in Fig. 5j: this is roughly constant at ~ 1.4 for the STO-3G basis but with triple-zeta bases it is 1.80 for NH$_3$, 1.10 for PH$_3$, and 1.17 for AsH$_3$. The large jump in the resonance energy explicitly involves double occupancy of σ^*_A. This effect was noted earlier in that the diabatic parameters for NH$_3$ evaluated using STO-3G and cc-pVQZ are very similar for all properties except J_D, the only property sensitive to the "Hubbard U" of the σ^*_A orbital. Further, the discontinuity in the reorganization energy λ_2 also flows from the orbital compression apparent in Fig. 8: the diabatic orbitals made by combining the lone-pair orbital n with σ^*_A, and bending the compressed orbital in one direction will lead to more bonding character whist the other direction will lead to more antibonding character, increasing the reorganization energy. The effect is not as pronounced as the resonance energy involves the interaction of two electrons within the same compressed orbital whereas the reorganization energy involves the interaction of the compressed orbital with its weakly perturbed environment.

g) Why XH$_3$$^+$ radical cations have different geometries and inversion barriers to XH$_3$ molecules.

As discussed earlier, the renormalization apparent in Eqn. (11) doubles the apparent resonance energies and reorganization energies whilst increasing the diabatic angle by a factor of $2^{1/2}$ on going from XH$_3$$^+$ to XH$_3$ assuming that the properties of the orbitals are unchanged. This arises owing to the increased number of electrons and the appearance of new coupled conical-intersection seams. However, the ionization process does result in a rearrangement of the remaining electrons and hence some changes to orbital properties are actually expected.

Table 8. Comparison of CCSD(T)/aug-pwCVQZ calculated properties of XH$_3$ neutral and XH$_3$$^+$ radical cation species, interpreted assuming that the diabatic angle controlling the limiting values down columns in the periodic table is a universal constant (see Table 6).

XH$_3$	Neutral				Radical cation			
	τ_e °	θ_e °	$\Delta E^\ddagger$ eV	$2J_u/\lambda_u$	τ_e °	θ_e °	$\Delta E^\ddagger$ eV	$2J_u/\lambda_u$
NH$_3$	22.0	106.8	0.23	0.81	0	120	-	1.05
PH$_3$	32.5	93.9	1.44	0.50	15.5	113.2	0.13	0.81
AsH$_3$	33.5	92.5	1.76	0.45	16.4	112.4	0.18	0.79
SbH$_3$	33.7	92.2	1.92	0.44	16.4	112.4	0.28	0.79
BiH$_3$	34.8	90.7	2.55	0.38	19.6	109.3	0.42	0.67
Limit	37.6	86.7			26.6	101.5		

Table 8 compares the CCSD(T)/aug-pwCVQZ calculated ground-state properties of the XH_3 molecules with those of the XH_3^+ radical cations. The radical cations tend in the limit of a very heavy central atom ($2J_u/\lambda_u \to 0$) to quite different bond angles, just as the theory predicts based on the absence of d the states in the radical cation (Table 6). However, the deduced values of $2J_u/\lambda_u$ are uniformly larger for the radical cations, indicating that the resonance energy is more sensitive to occupation than is the reorganization energy. This effect is most significant for NH_3^+ as for it $2J_u/\lambda_u = 1.05$ and so the ion is planar. So while the generic renormalization effect causes all ions to have larger HXH bond angles than their corresponding neutral molecules, the production of high-symmetry planar structures *requires* in addition changes in the orbital properties. The Rydbergization compression effect operates for this cation just as it does for neutral ammonia, making its properties distinctly different from those of the others, but this does not explain why $2J_u/\lambda_u$ increases for all molecules. Its explanation is related, however: the positive charge changes the orbital shapes to attract electrons closer to the nucleus, confining their volume. The effect is again larger at the planar geometry than at localized geometries, hence $2J_u/\lambda_u$ increases. Diabatic description of the bonding thus captures the chemical insight that goes into VSEPR theory, explains the orbital dependencies embodied into Walsh's rules,[53, 54] and quantifies how close any molecule is to being at the boundary between low-symmetry and high-symmetry structures.

We do not provide full quantitative analysis of the potential energy surfaces for the XH_3^+ radical cations, however, as within the valence-bond description more terms come into play than just those involving $n \to \sigma^*_A$ and these would need to be included. These terms involve $\sigma_A \to n$ excitation. Intuition from VSEPR theory indicates that vibronic couplings associated with this new excitation are small as it predicts the associated dications to be planar. Hence they are ignored in the previous discussion, and in Table 6.

5. Conclusions

Our general diabatic formalism for closed-shell chemical reactions is expanded by inclusion of Rydberg orbitals, allowing it to quantitatively analyze the results from high-level calculations of the ground and excited states of XH_3 molecules. Generally, this results in a 6-state 11-parameter diabatic model that simultaneously fits ground-state and excited-state potential-energy surfaces down to very small HXH angles of order 70°. In addition, our formalism offers a much simpler diabatic description in terms of a renormalized effective two-state model containing only 3 parameters. The two states used in this model are the ground-state g and its "twin state", in this case the double valence excitation d ($n \to \sigma^*_A$, $n \to \sigma^*_A$). The conclusions drawn from application of the model are:

(i) Reversal of Rydberg and valence orbital ordering. The most important feature revealed by the diabatic model is that the ordering of the lowest Rydberg orbital and the σ^*_A valence orbital interchanges between NH_3 and AsH_3, with the two being nearly degenerate for PH_3 but ordered more like AsH_3 than NH_3; for NH_3, the Rydberg orbital is the lowest in energy. As the diabatic model uses different functional forms for the properties of these orbitals, the near degeneracy for PH_3 produces homogenized orbitals and therefore presents a worst-case scenario for model application. The results obtained are still meaningful and useful, however.

(ii) Rydbergization and reassigned absorption spectra for NH_3

and PH_3. While the electronic-structure calculations used to parameterize these diabatic models are required to show balance between absolute accuracy and interpretability, their usefulness is demonstrated by the introduction of new spectral assignments for the VUV electronic absorption of NH_3. Bands in the one-photon absorption spectrum observed at 18.4 eV and at 30-33 eV previously assigned to double excitations involving Rydberg transitions are reassigned to the valence single-excitation resonances $n \to \sigma^*_E$ and a combination of $\sigma_E \to \sigma^*_E$ and $\sigma_E \to \sigma^*_A$, respectively. The 18.4 eV band had been previously assigned[114] as $n \to 3s, n \to ?$ and presumed to be associated with the IP observed at 24 eV that is assigned[119] to the double excitation $n \to 3s, n \to \infty$. Properties of the diabatic model are key to this reassignment as the $n \to 3s, n \to 3s$ excitation dr is found to be counter-intuitively at *higher* energies than $n \to 3s, n \to \infty$ and ca. *four* times the energy of r, the corresponding single excitation $n \to 3s$. This result arises because of the strong coupling between the Rydberg and valence states, an effect described by Mulliken as "Rydbergization",[70, 71] and the anomalous orbital ordering for NH_3. Our theoretical analysis also independently confirms previous experimentally based deductions[118, 120] that the lowest-energy transition in PH_3, which is commonly still labelled as a Rydberg absorption,[117] is in fact dominantly valence in nature.

(iii) The number of electrons occupying the interacting orbitals controls the number of critical conical intersections to rescale the magnitudes of the interactions and the extent of distortion produced. For the XH_3^+ radical cations, only the conical intersection between G and S critically controls structure, but for XH_3 the extra electron generates conical intersections between S and D and between G and D that qualitatively change the ground-state structure. This naively doubles the effective resonance couplings and reorganization energies and increases the diabatic torsional angle by a factor of $2^{1/2}$. Hence the HXH bond angles in the radical cations are always much larger than those in the corresponding neutral molecules.

(iv) Universality of the diabatic angle. The critical prediction of the diabatic model, that the fundamental nature of the diabatic orbitals is always preserved, is established for both XH_3 and XH_3^+ once the required parameter renormalization is taken into account. This hold well for molecules in which the valence state is lowest in energy, independent of X and calculation type. For XH_3 molecules we fit $\theta_{m2} = 101.1 \pm 0.5°$, very close to the value of $acos(-1/5) = 101.5°$ expected for maximum overlap with bonding orbitals orthogonal to sp diabatic orbitals. Deviations of a few degrees are found when the Rydberg orbital is lowest in energy, indicating that this scenario leads to a significant perturbation in the nature of the diabatic orbitals. As a result, the expected bond angles in the absence of resonance (i.e., the equilibrium structure expected as the row number in the periodic table becomes infinite) are therefore 101.5° for XH_3^+ and 86.7° for XH_3 (Table 6).

(v) $2J_2/\lambda_2$ controls structure and hybridization. This identification of one of the three parameters in the effective two-state model as a universal constant leaves only two parameters, say J_2 and λ_2, left to describe simultaneously the properties of the ground state g and its twin state d. Significantly, the value of the equilibrium ground-state equilibrium HXH bond angle θ_e then becomes controlled only by the ratio $2J_2/\lambda_2$. In the limits of $2J_2/\lambda_2 = 0$ and $2J_2/\lambda_2 \geq 1$ the XHX bond angles then become $\theta_e = 86.7°$ and 120°, respectively, using Eqns. (1) and (15), see Table 6. The EOM-CCSD/VTZ calculated values of $2J_2/\lambda_2$ quantitatively track the observed bond angles within this range, including reproduction of the anomalously large value for NH_3.

(vi) The size of the sp hybrid orbital controls $2J_2/\lambda_2$ and hence

weather molecules are planar or pyramidal. The values of J_2, λ_2, and hence $2J_2/\lambda_2$ are related to the size of the *sp* diabatic orbital of the central atom. The reorganization energies λ reflect the cost of interchanging one *sp* linear combination in a bonding configuration with the other, in the presence of the hydrogens. The resonance energies J reflect the interaction between an electron in one of the *sp* linear combinations with the other. Both properties clearly scale with *sp* orbital size but the resonance energy scales quadratically and hence $2J_2/\lambda_2$ also scales with size. When XH_3 molecules are ionized to make XH_3^+, the resulting orbital contraction towards the heavy-atom nucleus again increases this ratio, making it > 1 for NH_3^+, forcing this ion to be planar.

(vii) The Rydberg-valence orbital reordering produces a discontinuous change in sp hybrid orbital size. In any simple theory describing the ground-state structure of the XH_3 series, the most significant question of interest is the large difference between the bond angle of NH_3 and the other molecules. The diabatic model associates this discontinuity with an abrupt change in $2J_2/\lambda_2$, linking it quantitatively to the analogous discontinuity in the well depth and also to the discontinuity in the energies of the Rydberg excitations. Its origin stems from the inversion of the ordering of the Rydberg and valence orbitals that occurs for NH_3 that fundamentally changes the nature of the twin state (and hence the ground state) from one that is *stabilized* by Rydbergization in PH_3-BiH_3 to one that is significantly *compressed and destabilized* by it in NH_3. So while the cause of Rydbergization is the same in NH_3 and the other molecules, its manifestations are completely different. In this way, a close link is also established between the equilibrium structure and well depth in NH_3 and the properties of diabatically treated photodissociation reactions that directly exploit Rydbergization.[49, 50, 70, 71, 129]

(viii) Diabatic models unify molecular structural, kinetic, and spectroscopic properties. A tight connection is established between the ground-state structure and reactivity of these molecules and their spectroscopy, as has been achieved in the past using diabatic models only for electron-transfer reactions.[20] For example, this allows the details of the ground state surface out to 70°, including the equilibrium bond angle and well depth, to be determined purely from the properties of the excited states evaluated at the 120° planar D_{3h} geometry. A central concept of the diabatic approach is that key factors controlling ground-state properties can be determined through looking at excited-state properties, a technique not available to established chemical interpretation approaches such as VSEPR theory. Conversely, it is also possible to predict excited-state transition energies purely

from the shape of the ground-state surface.

(ix) Orbital following. Pauling's ideas concerning hybridization led to a revolution in chemical understanding[123, 124] by showing how *s-p* orbital mixing could produce shapes that pointed in the directions of bonds. The insight is that bonds form at specific angles to maximize overlap with these orbital shapes, a process known as *orbital following*.[69] While much of modern chemical understanding, including the VSEPR theory, is based on this principle, detailed calculations have shown that significant deviations often occur, especially for distorted structures.[69, 125] We see that the principle applies to equilibrium structures, making it useful in VSEPR theory and in hybridization analysis, and in our diabatic approach for determining the equilibrium bond angle in the absence of resonance coupling. The diabatic model then reproduces the deviations from orbital following found for non-equilibrium structures.

(x) Answer to the VSEPR riddle- what really is the characteristic XHX bond angle? Whilst we find intuition derived from VSEPR theory to be very helpful in understanding parameters in the diabatic model, the standard description of the XH_3 series by VSEPR is confused. The traditional approach was that molecules with 4 electron pairs were intrinsically tetrahedral (θ=109.5°) and that electronegativity differences between the atoms exploited angular size differences between bonding and lone-pair electrons to provide modification.[65] Indeed, a discontinuity in electronegativity is found between N and P that parallels the bond-angle discontinuity (Fig. 5a and 5o). VSEPR theory has now been modified to instead view the intrinsic geometry as octahedral,[66, 67] implying that the lone pair expands to fill all uncoordinated sites. However, actual bond angles are determined by evoking minimum ligand radii, completely bypassing the electronegativity argument for the XH_3 series (at least).[67]

So what is the intrinsic HXH angle, 109.5° or 90°? What about XH_3^+? The diabatic model gives simple answers to these questions: the parameter $\theta_{m2} = \mathrm{acos}(-1/5) = 101.5°$ is a universal constant, and the number of coupled electrons modulates this to indicate intrinsic angles of 101.5° for XH_3^+ and 86.7° for XH_3 (Table 6). By tuning the resonance energy to reorganization energy ratio, any value between these and 120° can be achieved. The unusual angle in NH_3 arises from the electronegativity-driven discrete change in the ordering of lowest Rydberg orbital and the σ^*_A antibonding orbital of NH_3, an effect that significantly changes the repulsion of electrons *within* an electron pair. Even for NH_3^+ this effect holds as the resonance energy is actually an orbital property *independent* of occupation. These dominant controlling effects are not included within VSEPR theory.

Appendix. Mathematical Symbols used.

Variable Class	Description	Variations
τ, θ	XH_3 improper torsional angle, HXH bond angle	τ, θ - general variables, simply related by Eqn. (1) τ_e, θ_e - adiabatic equilibrium values $\tau_{mG}, \tau_{mD}, \theta_{mG}, \theta_{mD}$, - local diabatic-model minimum angles if potential harmonic, Eqn. (6) τ_{m2}, θ_{m2} - fitted effective 2-state model parameters, Eqns. (11)-(12).
H	Electronic Hamiltonian matrix	$\mathbf{H^{3D}}$ - expressed in basis of delocalized diabatic states $\{G, S, D\}$ depicting the ground state (G), single excited state (S), and double excited state (D). $\mathbf{H^{3L}}$ - expressed in basis of localized diabatic states $\{L, C, R\}$ centred on the L (left) pyramidal structure, C (central) planar structure, and R (right) pyramidal structure.
$|\psi_s\rangle$, $|\psi_p\rangle$	X atomic orbitals	

Symbol	Name	Definition
J	Resonance integral	$J_2 = \frac{1}{2}\left\langle \psi_s + \psi_p \middle\| H \middle\| \psi_s - \psi_p \right\rangle\Big\|_{\tau=0}$ used in effective 2-state model, Eqns. (11), (12), (18); a quarter of the energy difference between g and d adiabatic states at $\tau = 0$. J_G, J_D - this allowing for differences between the G and D states, Eqns. (2) and (5).
λ	Reorganisation energy	λ_2 is the effective 2-state model parameter, Eqns. (11) and (12); a half of the energy difference between the g and d adiabatic states states at $\tau = 0$. λ_G, λ_D - local quantities allowing for differences between the G and D diabatic states, defined only for harmonic potentials, Eqn. 8.
$2J / \lambda$	General ratio controlling properties of diabatic model Hamiltonians	$2J_2 / \lambda_2$ for the effective 2-state model, ≥ 1 indicates if the molecule is planar, otherwise pyramidal; Eqns. (11) and (12). $2J_u / \lambda_u$ is the value fitted assuming the diabatic angles τ_{m2}, θ_{m2} are universal constants (Table 6). $2J_G / \lambda_G$ and $2J_D / \lambda_D$ are local quantities allowing for differences between the G and D diabatic states
k	Harmonic force constant	
k_4	Quartic force constant	
α	Linear vibronic coupling constant	$\alpha_G = \left\langle \Psi_G \middle\| \partial \mathbf{H}/\partial\tau \middle\| \Psi_S \right\rangle\Big\|_{\tau=0}$ $\alpha_D = \left\langle \Psi_D \middle\| \partial \mathbf{H}/\partial\tau \middle\| \Psi_S \right\rangle\Big\|_{\tau=0}$
β	Quadratic vibronic coupling constant	$\beta = \left\langle \Psi_G \middle\| \partial^2\mathbf{H}/\partial\tau^2 \middle\| \Psi_D \right\rangle\Big\|_{\tau=0}$, always set to 0 $\beta_S/2 = \left\langle \Psi_S \middle\| \partial^2\mathbf{H}/\partial\tau^2 \middle\| \Psi_S \right\rangle\Big\|_{\tau=0} - k$, always set to 0 $\beta_D/2 = \left\langle \Psi_D \middle\| \partial^2\mathbf{H}/\partial\tau^2 \middle\| \Psi_D \right\rangle\Big\|_{\tau=0} - \beta_S/2 - k$, always set to 0
γ	Cubic vibronic coupling constant	$\gamma_G = \left\langle \Psi_G \middle\| \partial^3\mathbf{H}/\partial\tau^3 \middle\| \Psi_S \right\rangle\Big\|_{\tau=0}$ $\gamma_D = \left\langle \Psi_D \middle\| \partial^3\mathbf{H}/\partial\tau^3 \middle\| \Psi_S \right\rangle\Big\|_{\tau=0}$
E_R	Unperturbed Rydberg state energy	$\left\langle \Psi_R \middle\| \mathbf{H} \middle\| \Psi_R \right\rangle$
Γ_R	On-site repulsion between two electrons occupying the Rydberg orbital	Energy of the double Rydberg excitation above the ground state DR less twice the difference between E_R and the ground0state energy
V_{RV}	Rydberg-valence interaction energy	$\left\langle \Psi_R \middle\| \mathbf{H} \middle\| \Psi_V \right\rangle$

Acknowledgments

Notes and references

a: International Centre for Quantum and Molecular Structure, College of Sciences, Shanghai University, Shanghai 200444 China; 86-15618155341; E-mail: Jeffrey.Reimers@uts.edu.au
b: School of Mathematical and Physical Sciences, University of Technology Sydney, NSW 2007 Australia
c: Department of Physics and Astronomy, University College London, Gower Street, London WC1E 6BT UK
d: School of Chemistry, The University of Sydney, Sydney, NSW 2006 Australia
e: School of Mathematics and Physics, The University of Queensland, QLD 4072 Australia
f: School of Molecular Biosciences, The University of Sydney, NSW, 2006 Australia

1. F. London, *Z. Phys.*, 1928, **46**, 455.
2. H. Eyring and M. Polanyi, *Z. Phys. Chem. Abt. B*, 1931, **12**, 279.
3. M. G. Evans and M. Polanyi, *Trans. Faraday Soc.*, 1938, **34**, 11.
4. J. Horiuti and M. Polanyi, *J. Molec. Catalysis A*, 2003, **199**, 185. Translation of *Acta Physicochimica U.R.S.S.* 1935, **2**, 505–532.
5. F. T. Wall and G. Glockler, *J. Chem. Phys.*, 1937, **5**, 314.
6. N. S. Hush, *J. Polymer Sci.*, 1953, **11**, 289.
7. F. London, *Z. Phys.*, 1932, **74**, 143.
8. L. D. Landau, *Z. Phys. Sowjetunion*, 1932, **2**, 46.
9. L. D. Landau, *Z. Phys. Sowjetunion*, 1932, **1**, 88.
10. W. F. Libby, *J. Phys. Chem.*, 1952, **56**, 863.
11. J. Weiss, *Proc. R. Soc. London, Ser. A*, 1954, **222**, 128.
12. R. Kubo and Y. Toyozawa, *Prog. Theor. Phys.*, 1955, **13**, 160.
13. R. A. Marcus, *J. Chem. Phys.*, 1956, **24**, 966.
14. V. G. Levich and R. R. Dogonadze, *Dokl. Akad. Nauk. SSSR Ser. Fiz. Khim.*, 1959, **124**, 123.
15. N. S. Hush, *Z. Elektrochem. Angewandte Physik. Chem.*, 1957, **61**, 734.
16. N. S. Hush, *J. Chem. Phys.*, 1958, **28**, 962.
17. N. S. Hush, *Disc. Farad. Soc.*, 1960, **29**, 113.
18. R. A. Marcus, *Discuss. Faraday Soc.*, 1960, 21.
19. N. S. Hush, in *Proceedings of the 4th Moscow Conference on Electrochemstry 1956*, English translation: Consultants Bureau, New York, 1961, p. 99.

20. N. S. Hush, *Prog. Inorg. Chem.*, 1967, **8**, 391.
21. C. Creutz and H. Taube, *J. Am. Chem. Soc.*, 1969, **91**, 3988.
22. J. M. Warman, M. P. d. Haas, M. N. Paddon-Row, E. Cotsaris, N. S. Hush, H. Oevering and J. W. Verhoeven, *Nature*, 1986, **320**, 615.
23. I. B. Bersuker, *Chem. Rev.*, 2001, **101**, 1067.
24. I. B. Bersuker, *Chem. Rev.*, 2013, **113**, 1351.
25. S. Zilberg, Y. Haas, D. Danovich and S. Shaik, *Angew. Chem., Int. Ed.*, 1998, **37**, 1394.
26. S. Shaik, S. Zilberg and Y. Haas, *Acc. Chem. Res.*, 1996, **29**, 211.
27. S. Shaik, A. Shurki, D. Danovich and P. C. Hiberty, *J. Am. Chem. Soc.*, 1996, **118**, 666.
28. S. Shaik, A. Shurki, D. Danovich and P. C. Hiberty, *Chem. Rev. (Washington, D. C.)*, 2001, **101**, 1501.
29. S. Zilberg and Y. Haas, *J. Phys. Chem. A*, 2011, **115**, 10650.
30. D. G. Truhlar and C. A. Mead, *Phys. Rev. A*, 2003, **68**, 032501.
31. P. Politzer, J. R. Reimers, J. S. Murray and A. Toro-Labbe, *J. Phys. Chem. Lett.*, 2010, **1**, 2858.
32. R. Valero, L. Song, J. Gao and D. G. Truhlar, *J. Chem. Theory Comput.*, 2009, **5**, 1.
33. J. Pu, J. Gao and D. G. Truhlar, *Chem. Rev.*, 2006, **106**, 3140.
34. V. K. Babamov, V. Lopez and R. A. Marcus, *J. Chem. Phys.*, 1983, **78**, 5621.
35. J. Aqvist and A. Warshel, *Chem. Rev.*, 1993, **93**, 2523.
36. D. N. Silverman, *Biochim. Biophys. Acta, Bioenerg.*, 2000, **1458**, 88.
37. A. Warshel, P. K. Sharma, M. Kato, Y. Xiang, H. Liu and M. H. M. Olsson, *Chem. Rev.*, 2006, **106**, 3210.
38. R. A. Marcus, *J. Chem. Phys.*, 2006, **125**, 194504.
39. S. Hammes-Schiffer and A. A. Stuchebrukhov, *Chem. Rev.*, 2010, **110**, 6939.
40. A. Sirjoosingh and S. Hammes-Schiffer, *J. Phys. Chem. A*, 2011, **115**, 2367.
41. A. Sirjoosingh and S. Hammes-Schiffer, *J. Chem. Theory Comput.*, 2011, **7**, 2831.
42. R. H. McKenzie, *Chem. Phys. Lett.*, 2012, **535**, 196.
43. M. S. Baranov, K. A. Lukyanov, A. O. Borissova, J. Shamir, D. Kosenkov, L. V. Slipchenko, L. M. Tolbert, I. V. Yampolsky and K. M. Solntsev, *J. Am. Chem. Soc.*, 2012, **134**, 6025.
44. R. H. McKenzie, *J. Chem. Phys.*, 2014, **141**, 104314/1.
45. H. A. Jahn and E. Teller, *Proc. Roy. Soc. A*, 1937, **161**, 220.
46. P. García-Fernández, J. A. Aramburu, M. Moreno, M. Zlatar and M. Gruden-Pavlović, *J. Chem. Theory Comput.*, 2014, **10**, 1824.
47. R. G. Pearson, *Journal of Molecular Structure: THEOCHEM*, 1983, **103**, 25.
48. G. Herzberg and E. Teller, *Z. Phys. Chem.*, 1933, **21**, 410.
49. Z. H. Li, R. Valero and D. G. Truhlar, *Theor. Chem. Acc.*, 2007, **118**, 9.
50. S. Nangia and D. G. Truhlar, *J. Chem. Phys.*, 2006, **124**, 124309.
51. C. C. Levin, *J. Am. Chem. Soc.*, 1975, **97**, 5649.
52. J. R. Reimers, L. McKemmish, R. H. McKenzie and N. S. Hush, *Phys. Chem. Chem. Phys.*, 2015, **in press DOI:10.1039/C5CP02236C**.
53. A. D. Walsh, *J. Chem. Soc.*, 1953, 2296.
54. A. D. Walsh and P. A. Warsop, *Trans. Faraday Soc.*, 1961, **57**, 345.
55. L. Song and J. Gao, *J. Phys. Chem. A*, 2008, **112**, 12925.
56. I. B. Bersuker, N. N. Gorinchoi and V. Z. Polinger, *Theor. Chim. Acta*, 1984, **66**, 161.
57. S. N. Yurchenko, R. J. Barber, J. Tennyson, W. Thiel and P. Jensen, *J. Mol. Spectrosc.*, 2011, **268**, 123.
58. X. Huang, D. W. Schwenke and T. J. Lee, *J. Chem. Phys.*, 2011, **134**, 044320.
59. C. Sousa-Silva, A. F. Al-Refaie, J. Tennyson and S. N. Yurchenko, *Mon. Not. R. Astron. Soc.*, 2015, **446**, 2337.
60. S. N. Yurchenko, M. Carvajal, A. Yachmenev, W. Thiel and P. Jensen, *Journal of Quantitative Spectroscopy and Radiative Transfer*, 2010, **111**, 2279.
61. S. N. Yurchenko, J. Breidung and W. Thiel, *Theor. Chem. Acc.*, 2005, **114**, 333.
62. M. B. Robin, *Higher excited states of polyatomic molecules*, Academic Press, London, 1974.
63. A. W. Potts and W. C. Price, *Proc. R. Soc. London, Ser. A*, 1972, **326**, 181.
64. O. T. K. K. K. N. Kato M and Y. Hatano, *J. Phys. B: At. Mol. Opt. Phys.*, 2003, **36**, 3541.
65. R. J. Gillespie and R. S. Nyholm, *Quart. Rev. Chem. Soc*, 1957, **11**, 339.
66. R. J. Gillespie and E. A. Robinson, *Angewandte Chemie International Edition in English*, 1996, **35**, 495.
67. R. J. Gillespie, *Coord. Chem. Rev.*, 2008, **252**, 1315.
68. M. Kaupp, *Angewandte Chemie International Edition*, 2001, **40**, 3534.
69. N. V. Cohan and C. A. Coulson, *Trans. Faraday Soc.*, 1956, **52**, 1163.
70. R. S. Mulliken, *Acc. Chem. Res.*, 1976, **9**, 7.
71. R. S. Mulliken, *Chem. Phys. Lett.*, 1977, **46**, 197.
72. H.-J. Werner, P. J. Knowles, F. R. Manby, M. Schütz, P. Celani, G. Knizia, T. Korona, R. Lindh, A. Mitrushenkov, G. Rauhut, T. B. Adler, R. D. Amos, A. Bernhardsson, A. Berning, D. L. Cooper, M. J. O. Deegan, A. J. Dobbyn, F. Eckert, E. Goll, C. Hampel, A. Hesselmann, G. Hetzer, T. Hrenar, G. Jansen, C. Köppl, Y. Liu, A. W. Lloyd, R. A. Mata, A. J. May, S. J. McNicholas, W. Meyer, M. E. Mura, A. Nicklass, P. Palmieri, K. Pflüger, R. Pitzer, M. Reiher, T. Shiozaki, H. Stoll, A. J. Stone, R. Tarroni, T. Thorsteinsson, M. Wang and A. Wolf, *MOLPRO, version 2010.1, a package of ab initio programs*, University of Birmingham, Birmingham, 2010.
73. H. J. Werner and P. J. Knowles, *J. Chem. Phys.*, 1985, **82**, 5053.
74. P. J. Knowles and H. J. Werner, *Chem. Phys. Letts.*, 1985, **115**, 259.
75. D. Hegarty and M. A. Robb, *Molec. Phys.*, 1979, **38**, 1795.
76. J. F. Stanton and R. J. Bartlett, *J. Chem. Phys.*, 1993, **98**, 7029.
77. T. Korona and H.-J. Werner, *J. Chem. Phys.*, 2003, **118**, 3006.
78. C. Møller and M. S. Plesset, *Phys. Rev. A*, 1934, **46**, 618.
79. K. Raghavachari, G. W. Trucks, J. A. Pople and M. Head-Gordon, *Chem. Phys. Lett.*, 1989, **157**, 479.
80. H. Nakatsuji, *Chem. Phys. Lett.*, 1979, **67**, 329.
81. M. Ehara, M. Ishida, K. Toyota and H. Nakatsuji, ed. K. D. Sen, World Scientific, Singapore, 2002, pp. 293.
82. M. J. Frisch, G. W. Trucks, H. B. Schlegel, G. E. Scuseria, M. A. Robb, J. R. Cheeseman, J. A. Montgomery, T. Vreven, K. N. Kudin, J. C. Burant, J. M. Millam, I. S. S., J. Tomasi, V. Barone, B. Mennuci, M. Cossi, S. G., R. N., G. A. Petersson, H. Nakatsuji, M. Hada, M. Ehara, K. Toyota, R. Fukuda, J. Hasegawa, M. Ishida, T. Nakajima, Y. Honda, O. Kitao, H. Nakai, M. Klene, X. Li, J. E. Knox, H. P. Hratchian, J. B. Cross, C. Adamo, J. Jaramillo, R. Gomperts, R. E. Stratmann, O. Yazyev, A. J. Austin, R. Cammi, C. Pomelli, J. W. Ochterski, P. A. Ayala, K. Morokuma, G. A. Voth, P. Salvador, J. J. Dannenberg, V. G. Zakrzewski, S. Dapprich, A. D. Daniels, M. C. Strain, O. Farkas, D. K. Malick, A. D. Rabuck, K. Raghavachari, J. B. Foresman, J. V. Ortiz, Q. Cui, A. G. Baboul, S. Clifford, J. Cioslowski, B. B. Stefanov, G. Liu, A. Liashenko, P. Piskorz, I. Komaromi, R. L. Martin, D. J. Fox, T. Keith, M. A. Al-Laham, C. Y. Peng, A. Nanayakkara, M. Challacombe, P. M. W. Gill, B. G. Johnson, W. Chen, M. W. Wong, C. Gonzalez and J. A. Pople, *Gaussian 09, Revision D.01*, Gaussian, Inc., Pittsburgh PA, 2009.
83. J. D. Bene and H. H. Jaffè, *J. Chem. Phys.*, 1968, **48**, 1807.
84. R. L. Ellis, G. Kuehnlenz and H. H. Jaffé, *Theoret. Chim. Acta*, 1972, **26**, 131.
85. M. C. Zerner, G. H. Loew, R. F. Kirchner and U. T. Mueller-Westerhof, *J. Am. Chm. Soc.*, 1980, **102**, 589.
86. J. Zeng, N. S. Hush and J. R. Reimers, *J. Am. Chem. Soc.*, 1996, **118**, 2059.
87. B. Tejerina and J. Reimers, 2008.
88. W. J. Hehre, R. F. Stewart and J. A. Pople, *J. Chem. Phys.*, 1969, **51**, 2657.
89. K. Raghavachari, J. S. Binkley, R. Seeger and J. A. Pople, *J. Chem. Phys.*, 1980, **72**, 650.
90. D. E. Woon and T. H. Dunning, Jr., *J. Chem. Phys.*, 1993, **98**, 1358.
91. T. H. Dunning, Jr., *J. Chem. Phys.*, 1989, **90**, 1007.
92. T. H. Dunning, Jr., *J. Chem. Phys.*, 1989, **90**, 1007.
93. R. A. Kendall, T. H. Dunning, Jr. and R. J. Harrison, *J. Chem. Phys.*, 1992, **96**, 6796.
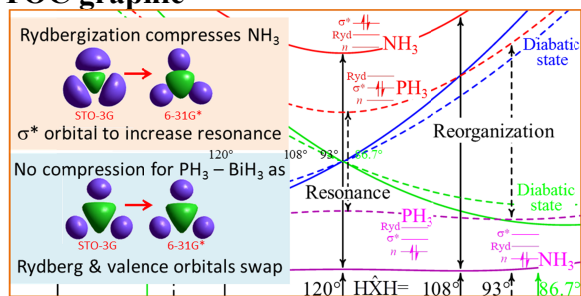94. D. E. Woon and J. T.H. Dunning, *J. Chem. Phys.*, 1993, **98**, 1358.

95. J. T.H. Dunning, K. A. Peterson and A. K. Wilson, *J. Chem. Phys.*, 2001, **114**, 2944.

96. K. A. Peterson, D. Figgen, E. Goll, H. Stoll and M. Dolg, *J. Chem. Phys.*, 2003, **119**, 11113.

5 97. D. Andrae, U. Háußermann, M. Dolg, H. Stoll and H. Preuß, *Theor. Chim. Acta*, 1990, **77**, 123.

98. N. J. DeYonker, K. A. Peterson and A. K. Wilson, *J. Phys. Chem. A*, 2007, **111**, 11383.

99. T. Van Voorhis, T. Kowalczyk, B. Kaduk, L.-P. Wang, C.-L. Cheng 10 and Q. Wu, *Annu. Rev. Phys. Chem.*, 2010, **61**, 149.

100. J. R. Reimers and N. S. Hush, *Chem. Phys.*, 2004, **299**, 79.

101. S. Larsson, *J. Am. Chem. Soc.*, 1981, **103**, 4034.

102. E. B. D. Wilson, J. C; Cross, Paul C., *Molecular Vibrations: The Theory of Infrared and Raman Vibrational Spectra*, McGraw-15 Hill Book Company, New York, 1955.

103. J. Swalen and J. Ibers, *J. Chem. Phys.*, 1962, **36**, 1914.

104. J. R. Reimers, L. McKemmish, R. H. McKenzie and N. S. Hush, *Phys. Chem. Chem. Phys.*, 2015, **in press 10.1039/C5CP02238J**.

20 105. L. McKemmish, R. H. McKenzie, N. S. Hush and J. R. Reimers, *Phys. Chem. Chem. Phys.*, 2015, **in press DOI:10.1039/C5CP02239H**.

106. L. K. McKemmish, R. H. McKenzie, N. S. Hush and J. R. Reimers, *J. Chem. Phys.*, 2011, **135**, 244110/1.

25 107. P. Schwerdtfeger, L. J. Laakkonen and P. Pyykkö, *J. Chem. Phys.*, 1992, **96**, 6807.

108. W. Klopper, C. C. M. Samson, G. Tarczay and A. G. Császár, *J. Comput. Chem.*, 2001, **22**, 1306.

109. W. Jerzembeck, H. Bürger, L. Constantin, L. Margulès, J. Demaison, 30 J. Breidung and W. Thiel, *Angewandte Chemie International Edition*, 2002, **41**, 2550.

110. T. Rajamäki, A. Miani and L. Halonen, *J. Chem. Phys.*, 2003, **118**, 6358.

111. C. Puzzarini, *Theor. Chem. Acc.*, 2008, **120**, 325.

35 112. R. Marquardt, K. Sagui, J. Zheng, W. Thiel, D. Luckhaus, S. Yurchenko, F. Mariotti and M. Quack, *J. Phys. Chem. A*, 2013, **117**, 7502.

113. J. Pesonen, A. Miani and L. Halonen, *J. Chem. Phys.*, 2001, **115**, 1243.

40 114. L. Ishikawa, T. Odagiri, K. Yachi, T. Nakazato, M. Kurokawa, M. Kitajima and N. Kouchi, *J. Phys. B: At., Mol. Opt. Phys.*, 2008, **41**, 195204.

115. W. Jerzembeck, H. Bürger, F. L. Constantin, L. Margulès and J. Demaison, *J. Mol. Spectrosc.*, 2004, **226**, 24.

45 116. C. C. Costain and G. B. B. M. Sutherland, *J. Am. Chem. Soc*, 1952, **52**, 321.

117. T. J. Xia, C. Y. R. Wu and D. L. Judge, *Phys. Scr.*, 1990, **41**, 870.

118. H. Friedrich, B. Sonntag, P. Rabe, W. Butscher and W. H. E. Schwarz, *Chem. Phys. Lett.*, 1979, **64**, 360.

50 119. E. M. Ishida M and H. Nakatsuji, *J. Chem. Phys.*, 2002, **116**, 1934.

120. W. H. E. Schwarz, *Chem. Phys.*, 1975, **9**, 157.

121. X. Zhang and J. M. Herbert, *J. Chem. Phys.*, 2015, **142**, 064109.

122. X. Zhang and J. M. Herbert, *J. Chem. Phys.*, 2014, **141**, 064104.

123. L. Pauling, *The Nature of the Chemical Bond*, 3rd edn., Oxford 55 University Press, 1960.

124. L. Pauling, *J. Am. Chem. Soc*, 1931, **53**, 1367.

125. J. P. Foster and F. Weinhold, *J. Am. Chem. Soc.*, 1980, **102**, 7211.

126. N. S. Hush, *NATO Adv. Study Inst. Ser., Ser. C*, 1980, **58**, 151.

127. J. P. Stewart, *J Mol Model*, 2007, **13**, 1173.

60 128. . *HYPERCHEM 8.0 Pro for Windows*, (2011) Hypercube Inc., Gainsville FL.

129. E. Evleth and E. Kassab, *Theor. Chim. Acta*, 1982, **60**, 385.

Physical Chemistry Chemical Physics Accepted Manuscript

Physical Chemistry Chemical Physics

ARTICLE TYPE

TOC graphic

Novelty statement:

The origins of the observed bond angles in XH_3 and XH_3^+ are explained using high-level calculations and a simple diabatic model.